ANALYSIS OF STAGNATION POINT FLOW OF NANOFLUID OVER A STRETCHING SURFACE

By

Sobia Sultana

NATIONAL UNIVERSITY OF MODERN LANGUAGES ISLAMABAD

February, 2024

Analysis of Stagnation Point Flow of Nanofluid over a Stretching Surface

By

Sobia Sultana

A THESIS SUBMITED IN PARTIAL FULLFILMENT OF THE REQUIREMENT FOR THE DEGREE OF

MASTER OF SCIENCE

In **Mathematics**

To

FACULTY OF ENGINEERING & COMPUTING

NATIONAL UNIVERSITY OF MODERN LANGUAGES ISLAMABAD

© Sobia Sultana, 2024

NATIONAL UNIUVERSITY OF MODERN LANGUAGES   FACULTY OF ENGINEERIING & COMPUTER SCIENCE

THESIS AND DEFENSE APPROVAL FORM

The undersigned certify that they have read the following thesis, examined the defense, are satisfied with overall exam performance, and recommend the thesis to the Faculty of Engineering and Computing for acceptance.

Thesis Title: Analysis of Stagnation Point Flow of Nanofluid over a Stretching Surface

Submitted By: Sobia Sultana   **Registration #:** 19/MS/Math/F20

Master of Science in Mathematics (MS Math)
Title of the Degree

Mathematics
Name of Discipline

Dr. Anum Naseem   _____
Name of Research Supervisor   Signature of Research Supervisor

Dr. Sadia Riaz   _____
Name of HOD (MATH)   Signature of HOD (MATH)

Dr. Noman Malik   _____
Name of Dean (FE&C)   Signature of Dean (FE&C)

Date: 27 February, 2024

AUTHOR'S DECLARATION

I <u>Sobia Sultana</u>

Daughter of <u>Muhammad Siddique</u>

Registration # <u>19/MS/Math/F20</u>

Discipline <u>Mathematics</u>

Candidate of **<u>Master of Science in Mathematics</u>** at National University of Modern Languages do here by declare that the thesis **Analysis of Stagnation Point Flow of Nanofluid over a Stretching Surface** submitted by me in fractional fulfillment of **MS Mathematics** degree,is my original work, and has not been submitted or published earlier. I also solemnly declare that it shall not, in future, be submitted by me for obtaining any other degree from this or any other university or institution. I also understand that if evidence of plagiarism is found in my thesis/dissertation at any stage, even after the award of a degree, the work may be cancelled and degree revoked.

Signature of Candidate＿＿＿＿＿＿

Name of Candidate: <u>Sobia Sultana</u>

<u>27th February, 2024</u>

ABSTRACT

Title: Analysis of Stagnation Point Flow of Nanofluid over a Stretching Surface

Nanofluids are heat transmission liquids with better thermo physical features and heat transfer capabilities that can improve the performance of several kinds of devices. Nanotechnology is significant in numerous categories, including heat transfer practices and energy applications. The present study examines the flow of Prandtl-Eyring nanofluid flowing over a stretching sheet placed in a porous medium. The fluid flow is developed in the presence of stagnation point and an inclined magnetic field. The heat and mass transfer characteristics in the flow regime are monitored using the Buon-giorno nano-model. The fluid model is presented in the form of partial differential equations and in order to convert these partial differential equations into ordinary differential equations, similarity transformations are utilized. Bvp4c method, a numerical technique is employed to solve the nonlinear ordinary differential equations. The effects of significant parameters on velocity, temperature and concentration profiles are illustrated graphically. The skin friction coefficient, Nusselt number and Sherwood number for the flow are calculated and examined numerically. The skin friction enhances for large values of magnetic and suction parameters and the opposite trend is encountered for the Nusselt and Sherwood numbers.

TABLE OF CONTENTS

LIST OF FIGURES

LIST OF TABLES

NOMENCLATURE

Symbols

x, y	Cartesian coordinates
u, v	Components of velocity
$U(x)$	Velocity of stretching sheet
M	Hartmaan number
Sh_x	Local Sherwood number
C_{fx}	Skin friction coefficient
Nu_x	Nusselt number
Re_x	Local Reynolds number
τ_w	Wall shear stress
q_m	Wall mass flux
q_w	Wall heat flux
T	Temperature
T_w	Surface temperature
T_∞	Ambient temperature
C	Nanoparticle concentration particle
C_w	Concentration at surface particle
C_∞	Ambient concentration particles
K	Thermal conductivity
σ	Electrical conductivity
B	Non-dimensional fluid parameter
A	Non-dimensional fluid parameter
α_I	Thermal diffusivity
$f(\eta)$	Dimensionless velocity
A	Material parameter
C	Material parameter
A	Stretching parameter

$\varTheta$	Non-dimensional temperature
H	Non-dimensional independent variable
φ	Dimensionless nanoparticle concentration
Le	Lewis number
Pr	Prandtl number
D_T	Thermophoresis diffusion coefficient
D_B	Brownian diffusion coefficient
Nb	Brownian Motion parameter
Nt	Thermophoresis parameter
ρ	Fluid density
T	Ratio between the effective heat capacity of the nanoparticle material and heat capacity of the fluid
B_o	Magnetic field strength
ψ	Stream function
μ	Dynamic viscosity
ν	Kinematic viscosity
H	Stagnation point parameter
Kp	Porosity parameter

ACKNOWLEDGEMENT

All glory and honor belongs to Allah Almighty, who made it possible for me to finish my thesis. I am grateful to the Allah Almighty and to my beloved and final prophet, Hazrat Muhammad (peace be upon him), who will always be a source of wisdom for humanity. I would like to extend my humble appreciation to my kind supervisor, Dr. Anum Naseem. She really improved my research skills and fully cooperated during my research and when I was writing my thesis.

I owe a lot of gratitude to my friends for their wise suggestions they provided when I was studying. It made easier for me to do my research and assisted me in gathering the supplies I needed to complete my thesis.

I want to express my sincere gratitude to my parents, brother, and sister in law, who have supported me throughout my life. Their love, prayers, and encouragement were essential to the success of my research work. Finally, I would want to extend my gratitude and blessings to everyone who helped me in any way during the thesis writing process.

DEDICATION

This thesis is dedicated to my wonderful parents, teachers, my brother and my sister-in-law who raised me to be the person I am today. I am grateful for your unconditional support, love, and guidance

CHAPTER 1

INTRODUCTION

1.1   Nanofluid

Nanofluid research is a very prominent scientific topic since it has numerous applications in many different sectors. Its applications range from microelectronics and oils to solar energy, electronics, compact heat exchangers, cooling of metallic plates, power transportation, mineral water, plastic sheet manufacture, rubber sheet manufacture and nuclear reactor design. Nanofluids utility demonstrate how important they are in advancing technology for industrial purposes. The development of a novel type of fluid termed as nanofluid, provides promising improvements to the efficiency of solar equipments. A novel fluid with much better heat transfer capabilities than the base fluid itself is created when solid nanoparticles known for their high thermal conductivity are combined with a base fluid possessing low thermal conductivity. This pairing provides improved thermal performance making it an important development for heat transfer applications. This type of fluid with particular qualities and features makes it a crucial for research in many fields of science and engineering. Water, ethylene glycol and oil are examples of basic fluids that are frequently used in nanofluids. Nanoparticles which are frequently made of metals, oxides, carbides or carbon nanotubes are mixed with these base fluids. Nanotechnology is a versatile and exciting area of research since the choice of particular base fluids and nanoparticles that allows modification in the characteristics to suit diverse applications. Nanofluids are highly useful for a variety of heat transfer applications due to their distinctive properties. The applications include home refrigerators, chillers, heat exchangers, grinding, machining, decreasing boiler flue gas

temperature, fuel cells, pharmaceutical operations, hybrid-powered engines, engine cooling and vehicle thermal management. The development of micro-scale liquid flow devices that offer compactness and a high surface-to-volume ratio, offering improved heat transfer compared to conventional flow systems has attracted a lot of attention due to breakthroughs in thermal science and engineering. These innovations are used in a variety of fields, including manufacturing, chemical engineering, aircraft and microelectronics. These industries can considerably increase heat transfer performance and efficiency by using nanofluids. As a result, managing thermal convection a key method of heat transfer has received considerable attention. Understanding and perfecting this process has received a lot of attention from researchers and scientists in order to improve heat transmission and overall efficiency in a variety of applications. The thermal conductivity of the heat transfer fluids has a significant impact on the effectiveness of thermal convection in heat transmission. The creation of energy-efficient heat transfer mediums is an advancement when compared with the low thermal conductivity of common fluids including water, oil and ethylene glycol. Enhancing these fluid's thermal conductivity is an important area for study and development because it has the potential to increase heat transfer effectiveness and make thermal convection more practical in a variety of heat transfer applications. Small solid particles can be added to fluids to alter their flow characteristics, thermal conductivity and transport qualities. The ability to create nanofluids with improved heat transfer properties as a result of this change makes them an improved means of enhancing thermal conduction and overall efficiency in a variety of applications. It is generally accepted that a base liquid's thermal conductivity can be increased by the addition of solid particles with sizes on the order of microns or millimetres. The widespread recognition and study of this phenomena has resulted in the creation of nanofluids with enhanced heat transfer capabilities and prospective usage in a range of heat transfer systems. The actual implementation of such solid additives is constrained due to the sedimentation of big atoms, obstruction of flow straits, destruction of pipelines & pressure decreases that result even if they may increase the heat transfer of the fluids. The two steps process is the peak often rummage-sale method for producing nano-fluids. Nanoparticles of several resources, such as nano fibers, nanotubes or additional nanomaterials are primarily created as nano sized particles ranging from 10-100 nm using different techniques. The nano sized triturate will next be dispersed in base fluids using strong magnetic force anxiety, high-shear mixing, ultrasonic agitation, homogenizing and ball refining. Nanoparticles incline to aggregate as a result of their and surface activity, large surface area, which has a bad influence on the solidity of nanofluid. The surfactant is further added to the nano-fluids to prevent this

effect. Choi [1] first studied nanofluids and led to an evolving era in fluid mechanics. The efficiency of the traditional fluids like air, fuel and water etc., can be enhanced through this advancement. He introduced tiny metallic particles into fluids and analyzed the thermo-physical properties of the suspensions. The work done by Choi attracted many researchers, among whom Lee *et al*. [2] provided evidences in favor of Choi's findings through experiments. These experiments confirmed upgrading of thermo-physical properties of nanofluids when compared to their traditional base fluids. The results revealed that if nano-sized particles possessing diameter less than 100 nm are added in the typical fluids, then the effectiveness of these fluids boosts nearly up to 40%. Xie *et al.* [3] analyzed influence of the interfacial nano-layer on the effective thermal conductivity of nanofluid. They deduced the formula for estimating improved thermal conductivity of nanofluid from the general solution of the heat conduction equation in spherical coordinates and they addressed the analogous hard sphere fluid model depicting the microstructure of particle/liquid mixes. They also studied the implications of nano-layer thickness, nanoparticle size, volume percentage and particle to fluid thermal conductivity ratio. Santra *et al.* [4] examined the cooling impact of copper-water nanofluid to imitate the behavior of laminar natural convection heat transfer in a square cavity that was differentially heated. They also studied the impact of copper particles in water with a solid volume fraction ranging from 0.05% to 5% for Rayleigh numbers 104 to 107. They discovered that for a given Rayleigh numbers, the heat transmission reduces with an increase in ϕ, whereas it rises with Rayleigh numbers for a given ϕ. Ghadimi *et al.* [5] studied stability of nanofluids since it played an important role in transfer of heat improvement aimed at future conceivable uses. It also signified generic stabilizations procedures as numerous sorts of solidity inspection tools. They also investigated the characterization analytical models and dimension methodologies of nanofluids prepared in a one or two step process. Hendraningrat *et al.* [6] analyzed nanofluid possibilities for Enhanced Oil Recovery (EOR) in low to high-permeability granite rocks and examined optimum absorption. They also investigated characteristics associated with the physical disjoining density mechanism, such as falling interfacial strains and changing wettability. They discovered that when hydrophilic nanoparticles were put into saline, interfacial tension (IFT) reduced. They looked at how interfacial tension (IFT) drops as nanofluid concentration increases, which shows the possibility of Enhanced Oil Recovery (EOR). Growing hydrophilic nano-particles reduces aqueous phase interaction angle and increases water wetness. They discovered that the advanced the nanofluid concentrations, greater the degradation of absorbency and porosity in Berea core sockets. Despite this, increasing the concentration of nanofluid results in decreased

interfacial tension (IFT) and altered wettability. They also highlighted the application of nanofluid Enhanced Oil Recovery (ERO). Mahian *et al.* [7] examined the computational and hypothetical influences on entropy formation and heat transmission for flow of nanofluids in various regimes and geometries. They offered many methods for calculating the thermophysical characteristics of nanofluids. They also analyzed about how flow of thermal nanofluid affects the pace of entropy generation in several functions. Sheikholeslami and Ganji [8] used the Discrete Time Model (DTM) to analyze the nanofluid problem with hydrothermal behaviours in the occurrence of fluctuating magnet field. They also took Brownian motion's impact on thermal conductivity into account and they compared the findings from the differential transformation method to earlier studies. They also looked at how the volume of nanofluid percentage, heat source parameter and Hartmann number affected movement of nano particles and heat transmission. Rehman *et al.* [9] explored entropy generation in non-Newtonian nanofluid flow using two important mechanisms of slip, thermophoresis diffusion & Brownian motion. These impacts were investigated using the momentum equation in conjunction with a lately developed equation for nano-particle dispersal. The conventional energy equation was adjusted for nano-fluid via include the impacts of nanoparticles. An entropy generation study for the current Jeffery nano-fluid model was discussed in order to assess the disorder in the thermodynamic system. Gireesha *et al.* [10] studied the three dimensional flow and non-linear radiative heat transfer of an Oldroyd-B nano-fluid flow across a stretched sheet with the impacts of a convective boundary conditions & uniform heat source/sink included. Tong *et al.* [11] studied the performance of a solar collector flat-plate employing H_2O, CuO and Al_2O_3 nanofluid as of working fluids. They examined and compared the entropy production, energy efficiency and energy destruction. The solar collector flat-plate had the best proficiency when Al_2O_3 was employed as working liquid (21.9% higher than when water was used). They investigated whether the use of Al_2O_3 and CuO nanofluids in the flat-plate solar collector could enhance thermal efficiency over the use of water, and they discovered that nanofluid 1.0%-Al_2O_3 provided the best performance. Agi *et al.* [12] investigated the physical characteristics of the synthesised Carbon Nanofiber based material (CPNP) as well as the effect of process factors. The rheology of the formed Cissus populnea nanofluid was examined and compared to that of Cissus populnea result and profitable polymer xanthan. Furthermore, the interfacial characteristics of CPNF were explored at various temperatures & concentrations, as well as the impact of salinity & their interface with ultrasound. Ahmadi *et al.* [13] investigated M5-tree, Multivariate Adaptive Regression Splines (MAR, Mixture Proportion Regression (MPR), Group Method of Data Handling (GMDH),

Artificial Neural Networks-Multi-Layer Perception (ANN-MLP) machine learning algorithms to estimate the μ of CuO-H_2O depending on nanostructure size concentration as well as temperature. The input formation obtained from numerous experimental studies was utilized to construct full model that could be used to a wide range of input variables. Furthermore, each variable's relative importance was assessed in order to identify the factors priority and their effects on dynamic viscosity. They used statistical measures such as R-squared value to compare the accurateness of models. The results of models indicated that employing the Artificial Neural Networks-Multi-Layer Perception (ANN-MLP) approach produces the most exact model. Based on these findings, for calculating the μ of the examined Artificial Neural Networks-Multi-Layer Perception (ANN-MLP) is a consistent approach. Further, they discovered that concentration has the largest relative value. Saffarian *et al.* [14] investigated the addition of employing nanofluid, varying the flow path in a flat dish solar collector to boost the convective heat transfer coefficient. To that aim, spiral pipes and U-shaped wavy pipes with similar pipe sizes are replicated on a flat dish collector. In volume fractions of 1% and 4%, CuO-H_2O and Al_2O_3- H_2O nanofluids are utilized. The consequences demonstrated that employing spiral pipes wavy rises the Nusselt number and skin friction significantly. They discovered that the pressure loss is highest for wavy pipes. Using nanofluid instead of water raises the skin friction in all circumstances. Excepting for CuO 4%, the Nusselt number has reduced in all cases owing to a significant rise in heat conductivity caused by the addition of nanoparticles to water. The drag force coefficient may rises to 78.25% and 4% by employing wavy pipes and CuO-water. Sheikholeslami and Farshad [15] examined the solar collector in terms of collector efficiency and irreversibility while taking fluctuating solar radiations into account. They evaluated these two elements as well as the performance component as primary purposes in order to get the optimal design. Ma *et al.* [16] examined the properties and applicability of several machine learning algorithms and addressed new advances in machine learning research in nanofluids. They furthermore explored machine wisdom methodologies for the study of nanofluid heat transfer in sustainable energy systems and renewable, as well as their potentials and limitations.

1.2   Stagnation Point

A stagnation point is a region in a flow field where the fluid's local velocity is zero. In all, but the most severe circumstances of fluid dynamics, a numerous examples of such points

appear in the form of the No-slip condition. Stagnation point flows created inside microfluidic interfaces have advanced significantly as a method for manipulating / trapping micro particles, characterizing materials and producing confined flows and isolated chemistries. Originally, these fluidic stagnation flows were used to characterize combinations & polymers. Though, in current years, these streams have taken on micro-fluidic forms, expanding their applications to encompass substrate patterning chip-integrated devices, single-cell analysis between others. When a body of fluid is immobile inside a certain place, this is referred to as fluidic stagnation. The local velocity of fluid at that point will be zero. Because it is inadequate to a dimensionless point, this area is frequently mentioned to as a stagnation point in certain types of flows. Alembert [17] developed the fluidic stagnation point notion for the first time in 1752, and employed on the concept of drag flow on compact boundaries. Fluidic stagnation was restricted previously to solid-liquid boundaries and branded as a disruption that could be evaded by designing airfoil with reasonably sharp leading edges. Two centuries later, in 1904, Prandtl [18] suggested the theory of boundary layer, which theorized frictional forces as the source of an actual thin fluidic film (stagnation point) spiking to an inflexible boundary and integrating heat transmission to a valuable instrument aimed at seizing and regulatory many micro-particles. Taylor [19] supported this breakthrough in 1934 by establishing the precise value of trapping substances with fluidic stagnation point flows, which consequently unlocked up a novel field of research attentive on attaching stagnation point streams for depicting polymers and emulsions. The study of stagnation point flow has received a lot of attraction because stagnation point flow is pervasive and includes interactions of various physical issues. Stagnation point flow is an essential phenomenon because all interactions between solid structures and fluid flow involve stagnation points or lines. It is mainly a flow near a solid surface. When the fluid approaches nearby a surface, it distributes into two main streams. The region of a stagnation-point reflects the largest mass deposition and rate of heat transport. Its applications cover a wide areas, few of which include wire drawing, electronic devices' cooling by fans, drawing of plastic sheets, polymer extrusion, nuclear reactors' cooling and numerous hydrodynamic processes involved in industry and engineering. Initially, Hiemenz [20] investigated a two dimensional stagnation point flow. Since then, the study on stagnation point has been a focus of scientists. Ariel [21] studied the laminar, continuous stagnation point flow of a viscoelastic fluid towards a moving plate and he also considered the instances of two-dimensional and axis-symmetric flow. Mahapatra *et al.* [22] investigated the properties of two dimensional and in addition stagnation-point flow with respect to a viscoelastic fluid across a deformable even surface in their work. The study took into account a situation in which the

surface stretched within its own plane and the fluid velocity was related to the distance from the stagnation point. Layek *et al.* [23] inspected heat transfer for a stagnation-point flow due to a stretching sheet which was assumed to be porous and the effects of internal heat absorption/generation modified the flow behavior. The unbroken stagnation-point flow of a two-dimensional second-grade viscoelastic fluid over a stretched surface with heat transfer was the subject of a study by Labropulu *et al.* [24]. According to the investigation, the fluid would lean against the wall. The authors showed that a resulted boundary layer was associated to surface's extending velocity and was smaller than the inviscid and free-stream velocity. The velocity at a given place was raised as fluid elasticity was increased. The scientists also found that a fall in temperature at a specific location is accompanied by an increase in fluid elasticity. Roşca and Pop [25] investigated stagnation point flow of stable combined convection across a vertical smooth plate with a second order slip when the plate is kept at a changeable heat flux. They discovered that in a given range of the velocity slip parameters and combined convection, the solutions to ordinary differential equations had two divisions, upper and lower subdivision solutions. Malvandi *et al.* [26] studied numerically the nano-fluid flow across a stretched surface. Navier's slip condition was used in distinction to the distinctive no-slide surface condition. The behaviour of three distinct water-based fluid nanoparticles namely TiO_2, Al_2O_3, Cu and was examined. They discovered that for adverse values of the unsteadiness parameter, a dual solution was found and that as it upsurged, skin friction increased while the rate of heat transfer decreased. The outcomes also showed that in contrast to the rate of stretching parameter, increasing the slip factor values extended the series of the parameter for unsteadiness. Besides, they discovered that increasing the stretching parameters, increased the heat transfer rate. Haq *et al.* [27] studied a nanofluid's stagnation point flow heat radiation properties and magneto hydrodynamics (MHD) above a stretching surface. They also acquired into description the mutual impacts of velocity and thermal slide. They investigated the state of zero flux for the added nanoparticles close to wall in case of stretchable flow phenomenon. Hayat *et al* [28] explored a viscous nanofluid's flow towards an irregular stretching surface with varying thickness. They also reported and compared analysis for both multi-wall and single-wall carbon nanotubes (SWNTs and MWNTs). Bano *et al.* [29] considered a viscous fluid's stagnation point flow with transfer of heat to a stretched cylinder. It was assumed that fluid moved indirectly on the cylinder's surface. They devised a model founded with the hypothesis that considered flow is axisymmetric in cylindrical coordinates. Ashraf *et al.* [30] investigated three-dimensional non-Newtonian nanofluid flow with radiation influence in a vertical cylinder. The flow analysis performed in the presence of a stagnation

point. Rosseland model was handled to calculate heat flux associated to radiation. They considered thermophoresis and Brownian motion aspects for describing nanofluid flow. Han *et al.* [31] presented the non-equilibrium molecular dynamic (NEMD) approach for describing the shock wave and the stagnation-point heat flow. They discovered that the heat flux is more sensitive to changes in the peak amplitude of the hypersonic flow in the bimodal velocity probability density function near the stagnation point. Reducing the peak amplitude of the hypersonic flow in the probability density function can efficiently minimize the stagnation-point heat flux. They compared the heat flow at the stagnation point by using three different types of exterior forms for the flying items. Khan *et al.* [32] investigated mass and heat allocation in non-axisymmetric Homann stagnation point flow caused by a linear stretchable sheet. The heat and mass transport phenomena was investigated using viscous nanofluid flow and chemical reaction. They used modified versions of Fourier and Fick's laws in mass and heat transfer mathematical modelling. Awan *et al.* [33] inspected the thermal study of an unstable flow of an incompressible second-grade fluid at its oblique stagnation point over an extended surface with sliding consequences. The study also demonstrated that the solutions were stable within a specific region of consistent parameters. They evaluated the Sherwood number declined with increased local second-grade parameter and the reduction in the value of the local second-grade parameter raised the value of the Nusselt number. The three-dimensional stagnation point flow across a cylindrical structure with a wavy shape was the subject of research by Riaz *et al.* [34] that took radiation into account. The authors also looked into two cases of stagnation point flow, one with a saddle point and the other with a nodal point. The radiative heat transport phenomenon was modelled using the nonlinear Rosseland approximation. Alhamaly *et al.* [35] looked into Stagnation point flow on a linearly expanding surface as well as heat transfer analysis with a nanofluid with varying characteristics. The stretched surface was assumed to extend radially in the analysis, whereas the enlarged surface heated convectively. The volume percentage of the nanoparticles and their distribution inside the flow's boundary layer were taken into consideration, along with the physical characteristics of the nanofluid.

1.3 Magnetohydrodynamics

Alfven [36] originated the term magnetohydrodynamics and established astrophysics as a separate scientific study. However, the formal birth of non-compressible

magnetohydrodynamic fluid occurred in 1936-1937. Hartmann and Lazarus [37] studied MHD fluid flow in ducts theoretically and experimentally. Magnetohydrodynamics is a fascinating substance of physics in which fluid dynamics utilizing magnetic influences can be inspected. The word magnetohydrodynamics is made up of three parts: "magneto" denotes a magnetic field, "hydro" denotes water, and "dynamics" denotes motion. Magnetofluid dynamics or hydromagnetics is the study of the magnetic properties and behaviour of electrically conducting fluids. Liquid metals (like mercury), electrolytes, plasma, and saltwater are a few examples of magnetic fluids. The idea of magnetohydrodynamics (MHD) is that magnetic fields can induce a current in a mobile conducting medium, which then causes fluid polarization and changes in the electromagnetic force. When it comes to the macroscopic behaviour of highly conducting fluids like plasmas or liquid metals, magnetohydrodynamics also known as hydromagnetics is concerned. This is accomplished by fusing hydrodynamics with Maxwell's equations. The plasma fluid is viewed as an electrically conducting medium in the context of ideal magnetohydrodynamics (MHD), and the governing equations include both Maxwell's equations and fluid dynamics equations. An electromagnetic field is inducted whenever a conducting material moves within an external field, producing an electric current in the process. Magnetohydrodynamics (MHD) is a field of study that focuses on relativistic research and has several applications. It is frequently used to represent dynamics, equilibria, and macroscopic force balance. Furthermore, perfect MHD is quite good at forecasting plasma stability. One intriguing point is that under optimal MHD, most catastrophic instabilities are unstable. MHD has been discovered to be relevant in laboratory plasmas, the solar environment and other fields, Earth's magnetosphere, the solar wind, the heliosphere, plasma turbulence in the inertial range, and neutron star magnetospheres are all described in detail by magnetohydrodynamics (MHD). In most astrophysical plasmas, MHD is a reasonable approximation. However, extensions are frequently required. The magnetic field and the surrounding fluid are strongly connected, flowing together in a way that can be defined as being "tied" or "frozen" to each other, according to the frozen-in flux theorem, a key idea in perfect MHD. Any two points in the system that are travelling with the bulk fluid velocity and are on the same magnetic field line will thus stay on that field line while the fluid flows around the points. The magnetic field's internal fluidic topology is fixed as a result of the fluid and magnetic field's interaction. The majority of electric current is condensed into thin, practically two-dimensional structures known as current sheets in many MHD systems. The presence of current sheets allows the fluid to be partitioned into magnetic domains with relatively weak internal currents. In contrast to the large magnetic domains that span thousands of kilometres, the estimated thickness of

current sheets in the solar corona ranges from a few metres to a few kilometres. Another example is the separation of different topological domains by current sheets in the magnetosphere of the Earth, which protects the ionosphere from the effects of the solar wind. The constant magnetohydrodynamic (MHD) flow, i.e., a flow for electrically conducting liquid over a partially infinite immobile plate in regards to radiation was studied by the researchers [38]. The authors also examined the numerical results for the temperature field and radiation parameter. With the occurrence of a constant vertically applied magnetic field, Turkyilmazoglu [39] scrutinized continuous magnetohydrodynamic (MHD) and laminar flow of considered electrically conducting liquid over radially stretchable spinning disc. The researchers also looked at a rotation parameter based on angular velocity and wall stretching. The vertical suction velocity, wall shear stresses, the pace of heat transmission and torque were estimated and described as physical characteristics of special relevance. A study on the three-dimensional flow of a viscous nanofluid in the presence of fractional slip and thermal radiation effects was done by Hayat *et al*. [40] they used Alumina as the nanoparticle while water employed as the base fluid. Waqas *et al*. [41] employed magnetohydrodynamics (MHD) to investigate the flow of a micropolar liquid in the direction of a nonlinear stretched surface. The analysis is provided using Joule heating, viscous dissipation and a convective boundary condition. Heat transport attributes were investigated using mixed convection theory. By using a parallel lattice Boltzmann method (LBM) algorithm, Ghasemi and Siavashi [42] explored the magnetohydrodynamic (MHD) flow with assumed natural convection of a *Cu- H$_2$O* nanoliquid in a squared shape porous enclosure. The effects of temperature-dependent viscosity and viscous dissipation were taken into account in the investigation. Additionally, they looked at how heat transmission and entropy production were affected by nanofluid concentration, Rayleigh number, Hartmann number and the ratio of porous-fluid thermal conductivity. The free convection boundary layer flows of an incompressible third-grade viscoelastic fluid across an isothermal inverted cone were studied by Gaffar *et al.* [43]. In a nonlinear, isothermal steady-state, the study involved effects of significant thermal radiation, heat absorption/generation and magnetohydrodynamics. The simulations presented were relevant to chemical engineering systems as well as the processing of low-density polymer materials. Shah *et al.* [44] considered the effect of a combined electric field and magnetic field in a spinning device on micropolar nanofluid among two parallel plates. They also looked at how Hall current affected the movement of nanofluid between two parallel surfaces. Moreover they assumed a steady-state flow of micropolar nanofluid. In order to analyze the stable, laminar, two-dimensional, magnetohydrodynamics and mixed convection flow within a square inclined

cavity filled with *Cu-H₂O* nanofluid, Ahmed *et al.* [45] used a finite difference method. A partial slip flow condition was imposed on the left and right vertical sidewalls of the cavity, which were considered to be adiabatic and moving upward in the investigation. The study made the assumption that the bottom wall would remain stationary and be uniformly heated in some areas, while remaining adiabatically heated in other areas and that the top wall would remain horizontal and remained cold. The research also took into account a central adiabatic blockage and externally applied magnetic field that was in actual parallel to fixed horizontal axis. Using magnetohydrodynamics, Yasmin *et al.* [46] examined mass and heat transport in the flow of non-Newtonian (micropolar) fluid. They believed that flow was generated by stretching a curved sheet with linear velocity. Khan *et al.* [47] considered the flow of borderline layer properties of magnetic widespread Newtonian molten liquid due to a parboloid revolt under chemical reactive species and bioconvection. They employed nanofluidic model in this study and incorporated thermophoresis and Brownian motion aspects. The thermophysical features of higher-order chemical processes and viscous fluid dissipation in nanofluids across a continually increasing porous surface were investigated by Gopal *et al.* [48]. They investigated the effects of a porous media with spatial coordinates. The time invariant, MHD and also incompressible nanofluid (Newtonian) flow was explored. A steady Williamson fluid flow in a microchannel was investigated by Shashikumar *et al.* [49] while taking electromagnetic force, Joule dissipation and viscous fluid dissipation into account. Peripheral convective conditions were applied on the borders. They discovered that the electromagnetic force has the potential to raise the Bejan number. Khan *et al.* [50] discussed the nanoparticles suspended in a viscous fluid. Further they assumed a 0% normal flux situation, this implies that there was no mass flow at the changeable thick surface. To govern the arbitrary motion of nanoparticles, an electromagnetic force was applied to the surface.

1.4   Porous Surface

Small gaps or pores that allow water, liquids, or vapour to pass through them are what defined as porous surfaces. Such surfaces enable the penetration of the object by outside elements including water, air and particles. Materials like paper, untreated wood, cardboard, sponge and cloth are examples of porous surfaces. Porous surfaces include things like decks, loose aggregate, boardwalks and soft porous surfacing. They are both sturdy and appealing, providing for significant design freedom. Porous asphalt, often known as open graded mix,

includes the identical ingredients as normal asphalt that eliminates the finest-textured materials. While, porous asphalt functions similarly to regular asphalt, precipitation can pass through the air holes to an underlying open graded, layer of impaired stone, wherever it gradually subverts into the subsoil. It has a rougher appearance than standard asphalt. Permeable interlocking concrete pavers are similar to ordinary pavers in appearance, but they include larger junctions or gaps at the turns that enable rainfall to flow into the junctions between the down and pavers through an open-graded foundation. These interlocking pavers, which are most typically used for walkways and parking lots, deliver a sturdy shallow for automotive transportation. Similar to gravel grids and porous grass, pervious flexible pavement systems are made of linked plastic cells (typically in the shape of cubes or cylinders) that are organized in a grid pattern to produce a flexible and supportive load-bearing surface. Porous surfaces are best suited for mild to moderate traffic regions. Less than 10% slope, capacity to manage runoff onto the site, at least two feet between the bottom of the drain rock and the top of bedrock and at least three feet between the bottom of the drain rock and the top of the water table are all site features that promote the use of porous materials. Porous surfaces are classified into two types: macroporous surfaces and microporous surfaces. Microporous surfaces have openings that are equivalent to the size of molecules. Microporous surfaces are used in gas separation, water management, the removal of metal pollutants, organic pollutants and oil recovery from process streams. Macroporous surfaces contain huge stomas that allow water and air to circulate freely. The base metal is showing during plating via apertures. The degree of sponginess is determined by the thickness of the plating, the manner of application, the roughness of the base metal and the cleanliness of the base metal. Porosity rises as plating thickness escalations. The separation of liquid droplets from porous material surfaces utilized in proton exchange membrane fuel cells was studied by Theodorakakos *et al.* [51] under the impact of cross-flowing air. On a specially designed transparent fuel cell, images taken with a charge-coupled device (CCD) showed that water produced in the Proton Exchange Membrane (PEM) builds up as droplets on the surface of the gas-diffusion layer. The droplets were carried away when the airflow velocity crossed a crucial line for a particular droplet size. The numerical model was used to get measurements of the dynamic and static contact angles in a transparent air-channel test model with three different carbon gas diffusion layer materials. Huan *et al.* [52] examined the surface variation of nickel titanium (NiTi) shape memory alloy by plasma electrolytic oxidation in sodium phosphate with the aim of producing porous nickel titanium (NiTi) surfaces for the application of biomedical. The oxidation was carried out potentiostatically and the stuffs of the subsequent

surfaces were associated to those produced under comparable situations in sodium metaphosphate or sodium aluminate. Haghighi and Or [53] investigated on thin surfaces with limited thermal capacity to demonstrate experimentally direct linkages between surface thermal fluctuation features and momentum-based turbulent eddy residence periods. For most practical applications, quick IR readings from a single sensor directed at the surface might be used. Theoretical connections between surface wetness and surface temperature changes enable remote measurement of drying and energy exchange processes from artificial and natural porous surfaces. Gu et al. [54] evaluated the accuracy of the axisymmetric drop form analysis technique and the half-angle approach for calculating contact angles on diverse solid surfaces. These surfaces comprised polished copper, polished silver, polished aluminium, polished titanium and porous copper. The study also looked at how surface properties affected the contact angle values. Numerical simulations of the evaporation of a droplet impacting a porous surface were carried out by Choi *et al.* [55]. In order to track droplet deformation, the study used a level-set formulation that took into account the combined effects of evaporation, heat transfer, mass transfer, porosity, porous drag and capillary forces. In another study, Eid *et al*. [56] considered the effects of suction / injection, heat radiation on considered two-phase flow of a general Carreau fluid across porous non-linearly expanding surface. The heat transferal properties for a nanofluid subjected to vertical tube with a porous media sandwiched between two transparent viscous fluids were investigated by Umavathi and Hemavathi [57]. The exploration included a form to comprehend the conduct of nanofluids while taking the volume percentage of solids into account. The effects of activation energy and porous space on the flow of nanofluid were investigated by Hayat *et al.* [58]. They used the relation of Darcy-Forchheimer to describe flow in porous space with changing porosity and permeability. They also took into account Brownian motion and thermophoresis. To improve hydrogen production in microreactors, Wang *et al*. [59] developed a unique micro-channel reactor and the reaction substrate was considered to be a porous surface. To study the gradient porous surface as well as two additional porous surface types (one with uniform pore size and two with gradient pore sizes) as catalytic supports, the researchers developed numerical models based on fractal geometry. All three microchannel reactors' fluid flow and heat transfer properties were sought out numerically while the fallouts disclosed that the micro reactor with the positively graded porous surface performed noticeably better overall than the others. In particular, it increased heat transmission by up to 18% and decreased pressure drop by up to 8%. Al-Farhany and Abdulsahib [60] investigated mixed convective heat transfer in a square enclosure with two levels and a rotating circular cylinder at the hollow's centre. In order to conduct the experiment,

an Al_2O_3-H_2O nanofluid was used for the top layer and a porous medium was superimposed for the bottom layer. The analysis made the assumption that the left and right walls would always be kept at high and low temperatures, respectively and that the above and lower horizontal walls would be insulated. Sajjad *et al.* [61] estimated the mere boiling transfer of heat coefficient for crusted porous surfaces using an AI-based technique. The proposed AI approach is capable of dealing with the complexities of coating parameters such as particle size, coating thickness and porosity. The formation of hydrates including activated carbon (AC) and the impact of porous surfaces on hydrate nucleation and development were both studied by Zhang *et al.* [62]. Rime-like hydrates, hydration fiber and hydrate chunks, which were formed at surface, bulges inner pores were the three different hydrate morphologies that were seen. Rapid hydrate nucleation resulted from the presence of surface micro-bulges and two-way convection within interior pores, which increased the gas-liquid contact area at the micro scale.

1.5 Thesis Organization

The thesis work is based on six chapters which are described below:

Chapter 1 is an introduction chapter in which the fundamentals of several ideas are covered.

The chapter 2 contains a deep and comprehensive literature review required for the ongoing research.

All of the fundamental terminology and ideas required for conducting an inquiry of the research work are covered in chapter 3.

Chapter 4 deals with the flow of a two-dimensional Prandtl Eyring nanofluid across a stretched surface. The heat and mass transport analysis has also been investigated. The system is described as a set of partial differential equations. Appropriate transformations play role in reducing governing differential equations to simplified differential equations, which are basically nonlinear. The bvp4c approach is adopted in regards to solve these substantial equations. The local Sherwood number along with friction drag and heat transfer rate are all figured out numerically.

In Chapter 5, a laminar flow of Prandtl-Eyring nanofluid flowing due to a porous stretched surface is examined. The assumed flow model is inspected in the existence of significant stagnation point and an inclined magnetic field. The hypothetical problem is represented by a complex system of differential equations. The concentration equation, energy

equation, and momentum equation are turned as ODEs and the results are revealed through bvp4c technique. The significant parameteric effects on velocity, in addition to temperature and also concentration profile is represented graphically. The coefficient of skin friction, local Nusselt number, and Sherwood numbers are computed.

CHAPTER 2

LITERATURE REVIEW

2.1 Nanofluid

Numerous engineering applications have embraced nanotechnology extensively as a viable option to save energy and lower the cost of building engineering infrastructure. Through the scaling down of nanoparticles to their nano-scale sizes and their absorption into fluids with low thermal conductivities, formation of nanofluids is acquired which is advantageous in a variety of ways. Because of their superior thermal properties nanofluids are widely employed as heat transfer fluids. Sajid *et al.* [63] investigated the behaviour of a spinning Prandtl Eyring nanofluid while accounting for factors such as MHD, chemical reaction, changing diffusivity of species, convective conditions, nonlinear radiations and velocity slip on a stretchy surface. They employed the Buongiorno model to simulate the effects of thermophoresis and the Brownian movement generated by nanofluid's presence. Kamran *et al.* [64] evaluated the heat transmission properties of a viscoelastic fluid in the existence of nanoparticles. Furthermore, viscous dissipation of fluid has been quantitatively enumerated in the equation of energy. They used the Buongiorno nanofluid model to investigate the properties of nanofluids. Hamad *et al.* [65] studied the Walters-B nanofluid travels in two dimensions across a vertically extending sheet containing motile microorganisms. They realistically extended Buongiorno's nanofluid model by using a adapted kind of Fick's and Fourier's theories in order to demonstrate the significant activation energy, radiative transfer of heat processes, and bio-convection on the flow problem under concern. Alqarni *et al.* [66] analyzed bio convectional second-grade nano liquid across three-dimensional flow a sheet with implications for thermal conductivity and

motile microorganism. Bouslimi *et al.* [67] employed slippage velocity, thermic radiation, convective boundary and sucking / injection condition to surge the heat transmission of Presumably Thermosiphon Solar Collector (PTSC) in the presence of the magnetic force. Entropy was measured in a leaky substance of Sutter by nanofluid flowing across an ascendingly parallel plate containing PTSC. They employed nanofluids of two types: silver-sodium alginate and copper-sodium alginate. Waqas *et al.* [68] explored the flow dimensions and microorganisms transfer of mass qualities in order to make their research more successful, inexpensive and better for the benefit of humanity. They assumed the effects of bio-convection through a tiny needle for Casson nanofluid. They investigated a changing magnetic field as well as temperature-dependent viscosity. The effects of nonlinear thermal rays and activation energy were also considered. Bayareh [69] used single-phase and two-phase techniques to investigate heat transfer of non-Newtonian nanofluids flowing in macro- and micro-channels. Mustafa *et al.* [70] studied MHD and mixed convection effects to investigate unstable nanofluid flow across a cone. The variable viscosity and viscous dissipation's effect were also taken into account in the study. Aljaloud *et al.* [71] investigated the thermal impact of cross nanofluid with bioconvection applications. The thermal influence of radiated phenomena, activation energy, and viscous dissipation were all supported. The flow was caused by the stretched cylinder. Hussain *et al.* [72] investigated the influence of MHD on steady three dimensional tangent hyperbolic nano fluidic flow via an extended surface containing gyrotactic microorganisms by addressing novel mass flux conditions. Li *et al*. [73] studied the flow of a ternary nanofluid past a stretching sheet subjected to temperature jump as well as Troian and Thomson slip conditions. The ternary nanofluid is created by suspending three different types of nanoparticles such as Ag, TiO_2 and Cu in water which acts as a base fluid and causes the nanoparticles to move. Silver's strong chemical stability and thermal conductivity were the primary reasons for its inclusion as the third nanoparticle in the hybrid nanofluid Copper-Titanium dioxide / water. Furthermore, they presumed the existence of heat source/sink and a radiation such that the resulting energy equation can be similar to the majority of real-world situations. Modi *et al.* [74] investigated the impact of nanofluid type, nanoparticle concentration and nanofluid depth on the performance of solar stills by using cutting-edge literature. They also discussed most recent literature on the use of nanofluid in solar still supplemented with the various augmentations. They also investigated the perception of hybrid nanofluid and its advantages over mono-nanofluid using various literatures, as well as its use in solar stills. A well-known numerical-based neuro-evolution heuristic approach was used by Butt *et al.* [75] and involved feed-forward neural networks that were trained using a blend of

genetic algorithms and sequential quadratic programming. The objective was to provide a descriptive analysis of heat-induced Prandtl-Eyring nanofluid flow on a stretchy sheet. By altering the material parameters, temperature difference parameter, heterogeneous reaction parameter, Prandtl number, stretching parameter, Schmidt number and Biot number, numerical results were produced using these techniques. The study found that lowering the temperature of the nanofluid had a similar impact as growing Prandtl number and also the values of material parameters. When the temperature difference parameter and the Biot number were applied, this impact was opposite. The study found that a drop in nanofluid concentration occurred when the Schmidt number, heterogeneous reaction parameter and temperature difference parameter were increased. Recently a lot of researches have directed their analysis towards nanofluids [76-84].

2.2   Stagnation Point

In many engineering and industrial applications, the study of stagnation-point flow for viscous or non-Newtonian fluids is crucial. Designing radial diffusers and thrust bearings, applying transpiration cooling, reducing drag, and improving thermal oil recovery procedures all require an understanding of stagnation point flow. Rehman *et al*. [85] explored the interaction between torsional spinning cylinders and radial stagnation point flow by observing the behaviour of a linearly twisting cylinder submerged in a heated viscous nanofluid. Mabood *et al*. [86] investigated non-linear heat radiation and chemical reactivity's effect on the oblique stagnation point flow of a viscoelastic nanofluid across a stretchable cylinder. The well known Buongiorno's model was used in the inquiry to take Brownian motion and diffusion of thermophoresis into account. Ahmed *et al*. [87] investigation focused on the Maxwell nanofluid's rotational stagnation-point flow over a porous rotating disc that was either stretching or contracting radially. An enhanced version of Buongiorno's nanofluid model was used by the researchers to track the Brownian and thermophoresis mobility of nanoparticles. The effects of changing the heat sink / source parameters and thermal conductivity on the heat transferal physiognomies for nanofluid were scrutinized by the researchers. Khan *et al.* [88] discussed the properties of dual sos lutions of an unstable stagnation-point flow for hybrid nanofluid subjected to spinning disc with the impression of Hall current. They represented solution in two branches. Upper branch and lower branch. They observed due to the hybrid

nanofluid, the radial velocity rises while the azimuthal velocity drops. However, the temperature rises owing to the hybrid nanofluid. The temperature and azimuthal velocity in the upper branch solution both drop as the magnetic parameter increases. In contrast, the transverse component of velocity initially raised and then fell for the lower branch solution, while the temperature enhansed continuously and monotonically. Vijay and Sharma [89] looked at the motion of a temperature-dependent viscous Maxwell nanofluid flowing over a rotating disc with the magnetohydrodynamic (MHD) and stagnation point. The Soret-Dufour impacts on the concepts of energy and concentration conservation were taken into consideration in the investigation. Additionally, the activation energy of the Arrhenius theory was used to depict the heat and mass transport behaviour. Khashi'ie *et al.* [90] studied the flow of an unstable separated stagnation point (USSP) on a Riga plate under heat production and electro-magnetohydrodynamic circumstances. *Cu* and *Al$_2$O$_3$* nanoparticles make up the fluid. However, they observerd when heat generation was considered for the boundary layer, heat transmission was slowed. Additionally, for greater values of the parameters of electro-magnetohydrodynamic, the domain of the solutions was increased and these solutions were dismissed at specified points of the parameter for unsteadiness. They furthermore observed that the streamlines in the first solution function as a regular stagnation point flow, but the streamlines in the second solution divide into two zones, demonstrating the occurrence of retrograde flow. Finally, utilization of stability examination, the initial solution remains as stable whereas for second solution, it was discovered to be unstable over time. Murad *et al.* [91] examined the behaviour of Casson-Carreau fluid heat transfer with thermal radiation over a continuous moving sheet near the stagnation point with magnetohydrodynamics (MHD). The study showed that for both Casson and Carreau fluids, a rise in the Weissenberg number leads to an improvement in the temperature profile and a decrease in the velocity profile. On the other hand, increasing the parameter of Casson fluid, shrinkage parameter and magnetic parameter values reduced the thermal distribution while improved the velocity profile. Additionally, the temperature profile for Casson and Carreau fluids lessened when increased the Prandtl number and parameter of radiation. Zainal *et al.* [92] emphasized the flow of stagnation point *Cu-Al$_2$O$_3$ / H$_2$O* hybrid nanofluid flow with thermal radiation and Arrhenius kinetics through a shrinking / stretching sheet. They moreover introduced a unique hybrid nanofluid. Vishalakshi *et al.* [93] considered the specific case of stagnation point flow with MHD of a *G-H$_2$O* nanofluid flow for the stationary value of Prandtl number that was 6.2. Makhdoum *et al.* [94] investigated the flow of *Al$_2$O$_3$* and *H$_2$O* nanofluids tempted due to permeable extending surface subjected to the effect of a Lorentz force and viscous dissipation.

Entropy production on nanofluid flow of stagnation point through heat absorption / generation impacts with suction. Taking into account the all encompassing influence of slips, Yu *et al.* [95] carried out a numerical analysis with the presence of double solutions in heat transfer and three-dimensional and also stagnation point flow within a porous material. To improve the heat transmission process nanofluids were used. A vertical surface at a stagnation point flow was the subject of an investigation by Islam *et al.* [96] for the unstable double-diffusive mixed convection boundary layer nanofluidic flow. The study made use of Buongiorno's model, which took thermophoresis and Brownian motion into account. The diffusion of regular and cross components were also taken into account while calculating thermal energy. When applying a second-grade micropolar fluid through a porous material in the direction of a stretched surface, Naveed *et al.* [97] took into consideration the magnetic field effect that was produced. On the sheet's surface, the investigation used stratification boundary conditions. In order to explore heat and mass transport, the researchers also looked into generalized Fourier and Fick's laws with activation energy. From more precise estimations, they noticed that the velocity profile was decreased as a result of the growth of the resistance effect. Furthermore, the fluid's angular velocity improved when the micropolar parameter's was increased.

2.3   Magnetohydrodynamics

Magnetohydrodynamics (MHD) is a fundamental concept in many branches of physics, including solar physics, astrophysics, plasma physics and others. The study of MHD in the sun is of particular importance. The impact of magnetic fields on the behaviour of dynamic conducting fluids are at the heart of MHD physics. A key idea in magnetohydrodynamics is that magnetic fields can cause electric currents to flow through dynamically conducting fluids, polarizing the fluid and causing changes in the magnetic field in the process. The underlying theory of magnetohydrodynamic and its applications in understanding diverse dynamic processes in the solar corona were thoroughly studied by Pontin *et al.* [98]. These phenomena include solar wind, jets, flares, coronal heating and coronal mass ejections. Aspects like acceleration, collisionless reconnection, non-thermal particles and recombination in systems outside the corona were also explored in the study. An incompressible, viscous and electrically conducting fluid's for unsteady magnetohydrodynamic (MHD) free convection mass and heat transfer flow was studied by Bafakeeh *et al.* [99]. The fluid flowed through a vertical plate within a porous media while

the study took into account the presence of thermal radiation and chemical reactions. The impacts of Soret, rotation, and Hall current in the system were also investigated by the researchers. A mathematical model was created by Safdar *et al.* [100] to theoretically and statistically analyze the stable magnetohydrodynamic (MHD) Maxwell nanofluid flow over a porous stretched sheet containing microorganisms with gyrotactic behaviour. In order to stabilize the suspended nanoparticles caused by bioconvection caused by buoyancy forces, the study used microorganism theory. With regard to the diffusion of liquid hydrogen and oxygen, Patil & Kulkarni *et al.* [101] investigated the magnetohydrodynamic triple diffusive coupled convective Eyring-Powell nano liquid flow across a vertical plate in motion. Using two alternative heat transfer scenarios, one with a predetermined exponential order surface temperature and the other with a mandated exponential order heat flux, the study was performed. Amjad *et al.* [102] searched tangent hyperbolic nanofluidic flow over an exponentially stretched sheet. Tangent hyperbolic nanofluid was used by the researchers to cool electronic components, which produced a lot of heat when operating with slip at the walls, the magnetohydrodynamic Jeffery-Hamel flow was studied by Boujelbenea *et al.* [103] under the influence of an angled Lorentz force. Numerous applications, such as geothermal systems, electronic cooling devices and current energy systems, frequently included this kind of flow. The goal of the study, in accordance with the second law of thermodynamics, was to achieve two dimensional, entirely radial flow in a converging-diverging channel. Rashid *et al.* [104] investigated the movement of a hybrid nanofluid made up of silver (*Ag*) and alumina (*Al*) nanoparticles in water across a revolving disc. The impacts of thermophoresis, Brownian motion, activation energy and electromagnetic field were among the elements that were considered in the study. Waini *et al.* [105] highlighted the findings of the radiative flow, MHD investigation and non-Newtonian Reiner-Philippoff nanofluid thermal characteristics with thermophoresis diffusion and Brownian motion effects. The Buongiorno hypothesis served as the foundation for the model under investigation. This one-of-a-kind simulation was designed to identify both shear thinning and shear thickening properties in that fluid with thermophoresis and Brownian motion effects. To investigate the flow of Maxwell nanofluid, which consisted of both nanoparticles and microorganisms, over a stretched surface, Alrabaiah *et al.* [106] performed a semi-analytical magnetohydrodynamic simulation. A bi-directionally linearly stretched surface was the main object of the inquiry for nanofluid flow. The flow of the Maxwell nanofluid was examined in relation to chemical reaction, Soret and Dufour numbers. In addition, the research investigated the thermal and mass transport processes using the Cattaneo-Christov well known model. Ragulkumar *et al.* [107] studied the MHD water-

based nanofluid flow using an upright cone. This mathematical model used the heat and mass flux patterns to investigate MHD, viscous dissipation, radiation, chemical reactions and suction / injection processes. Mahmud *et al.* [108] investigated the MHD oblique flow approaching a revolving disc. They also considered the effects of heat transport and hydromagnetics. Abbas *et al.* [109] explored an unstable, incompressible fluid model and compared the outcomes of stretching cylinder and sheet, as well as the effects of Darcy resistance and viscous dissipation. They took into account thermal radiation, thermal slip and induced magnetic field in the presence of liquid thermal conductivity as a variable. Zeeshan *et al.* [110] looked at the effects of mass and heat transfer, thermal radiation, an induced magnetic field and viscous dissipation phenomena on the time-dependent magnetohydrodynamic flow for a reactive fluid across a vertically slanted plate. A boundary layer estimate was used to design a movement that precisely represents the time-dependent equations for energy, momentum, continuity, concentration, magnetic induction. They looked at the porous rotating channel's with uneven heat source and chemical reaction. High thermal radiation was thought to occur with increasing temperature and concentration. The intermolecular forces (IMF) impact was seen to down for high magnetic Prandtl numbers. They also discovered that raising the heat source factor increased fluid velocity.

2.4   Porous Surface

A porous surface is often referred to as a porous substrate. A porous surface allows moisture to enter matter, causing various forms of corrosion, such as corrosion beneath insulation. The physical properties of magnetohydrodynamics (MHD) Carreau nanofluid flow with bi-convection across an upper paraboloid porous surface were examined by Shahid *et al.* [111]. They also looked for activation energy and chemical reactions. Algehyne *et al.* [112] investigated thermal transport in a Maxwell hybrid nanofluid passing through an infinite stretchable vertical porous sheet. They also studied the thermal characteristics of hybrid nanofluid that was included in the study. In the presence of a continuous magnetic field, Arshad *et al.* [113] investigated the flow of a viscous nanofluid with heat and mass transfer over a porous flat surface. The impacts of Brownian motion, thermophoresis and viscous dissipation in the system were also studied by the researchers. Shah *et al.* [114] investigated the phenomena of an inclined stretching sheet generating a slip flow of upper convected Maxwell (UMC) nanofluid via a porous media and a magnetic field. To characterize the mass and heat

transmission processes, they used the diffusion model developed by Cattaneo and Christov. They constructed the relaxation framework of a viscoelastic system by using the Cattaneo-Christov model for upper convected Maxwell (UCM) nanofluid to calculate both heat and mass transmission. Thermophoresis, Brownian motion, and heat generation effects in the presence of a chemical reaction were accounted. Usafzai et al. [115] explored the effects of second degree velocity slip and thermal jump circumstances on water-based nanofluid flow and heat transfer through a permeable bidirectional moving surface in a porous medium environment Ullah et al. [116] studied the temperature dependent thermal conductivity, surface heat flux and magnetohydrodynamic effects on electromagnetic fluid across the magnetically vertical surface placed in a porous material. Khan et al. [117] numerically investigated the magnetohydrodynamics boundary layer flow of a Casson fluid in rotating frame via porous material generated by exponentially extending surface. Awan et al. [118] studied a hybrid nanomaterial AA7072-AA7075-based fluidic system along a porous surface using an artificial neural network with Bayesian regularisation scheme (ANNs-BRS) in order to account for magnetohydrodynamics (MHD), Abass et al. [119] dealt with the bio-convective heat transferal of a Williamson nanofluid over an inclined moving plate submerged in a porous medium. They noticed that higher flow velocity is caused by an increase in the buoyancy ratio parameter. They also discovered that a higher Weissenberg number results in greater flow intensity, but a higher bioconvective Rayleigh number has the reverse effect. They also saw how fluid particles moved as a result of Brownian motion. Zhags et al. [120] examined the combined impact of ion-specific interactions and porous surfaces on hydrate formation kinetics. The study was conducted in the presence of four halogen salts. The scientists discovered that the hydrate formation was simultaneously promoted and inhibited by the ion-porous surface system. A concentration of 0.05 weight percent of potassium iodide totally eliminated the hydrate induction period, making it the most effective halogen salt in promoting hydrate nucleation. Tran et al. [121] discussed the fundamental knowledge and features of wetting ridges, as well as the most recent advancements that allow for the precise research and suppression of wetting ridge formation on Slippery liquid-infused porous surfaces. Furthermore, they provided their thoughts on new and interesting avenues for Slippery liquid-infused porous surfaces. Dhivagar et al. [122] investigated a unique conch shell biomaterial as an energy storage material and porous medium in a solar still to increase system performance. When the solar radiation is low, the conch shell biomaterial retains the heat energy of the sun and releases it into the salty water. Furthermore, the porous surface of the conch shells

functions as a porous absorber, absorbing a huge quantity of solar energy and raising the water temperature.

CHAPTER 3

DEFINITIONS

This chapter contains a number of often used principles and definitions to assist readers in understanding the analysis in the following chapters.

3.1   Fluid

A fluid [123] is referred to as a material that constantly deforms when it experiences applied shear stress, or some external force. Fluids are liquids, gases, and plasma. Some solids, however, act like fluids. For example, pitch is a solid with a high viscosity that flows (very) slowly. Solids are not fluids in general because they withstand tangential stress and only deform to a point.

3.2   Fluid Mechanics

Mechanics is a physical science that studies things that are either moving or motionless and are subjected to an external force. There are two primary branches [123].

3.2.1 Fluid Statics

Fluid statics [123] or hydrostatics is the branch of fluid mechanics that studies fluids at rest. It embraces the study of the conditions under which fluids are at rest or in stable equilibrium; and is contrasted with fluid dynamics, the study of fluids in motion.

3.2.2 Fluid Dynamics

Fluid dynamics [123] is the sub-discipline of fluid mechanics that deals with the study of how fluids (liquids and gases) behave and interact with their surroundings. It is a branch of classical physics and has numerous applications in engineering, meteorology, oceanography, aerospace, and many other fields.

3.3 Stress

The quantity of force applied to an element divided by the cross-section area of the element on which the force operates is defined as stress. The element deforms when the deforming force is given to it. To return to its original size and shape an opposing force will be produced within it. The term "stress" refers to the amount of restorative force per unit area of material [124].

$$\sigma = \frac{F}{A}.$$
(3.1)

Application of stress are structural engineering, mechanical design and aerospace engineering, in addition geotechnical engineering and manufacturing processes. In the SI system, stress is measured in Pascal (Pa).

There are two types of stress.

3.3.1 Shear Stress

It is defined as a force which is tangentially applied upon the plane's surface area. When forces acting on surface are applied parallel to the surface, and this stress acting on the surface tracks tangent, then the form of stress is designated as shearing stress [124].

$$\text{Shear stress} = \frac{\text{Force}}{\text{Surface Area}}. \tag{3.2}$$

3.3.2 Normal Stress

The normal [124] stress is the kind of stress that results from applying an axial force to a component. To put it another way, when the stress applied to the body is perpendicular. In the SI system, normal stress is measured in mill Pascal's (MPa).

$$Normal\ stress = \frac{\text{Axial Force}}{\text{Cross Sectional Area}}. \tag{3.3}$$

3.4 Strain

Strain [124] is a concept used in mechanics and materials science to quantify the deformation of a solid body when subjected to external forces or loads. It represents the relative change in shape or size of the body due to the applied stress. Strain is a dimensionless quantity expressed as a ratio or percentage and is a measure of how much the body has stretched, compressed, or deformed.

3.4.1 Shear Strain

Shear strain [124] also known as tangential strain, is a type of strain that describes the deformation of a solid body when subjected to a shear stress. It represents the relative change in shape of the object due to forces applied parallel to its surface, causing the body to distort without a change in volume.

3.4.2 Normal Strain

Normal Strain [124] also known as axial strain or linear strain, is a type of strain that describe the relative change in length of a solid body along a specific axis or direction. It is a measure of how much the body has elongated or contracted under the influence of an applied force or stress.

3.5   Viscosity

Viscosity [124] is a fundamental property of fluids that describes their resistance to flow or deformation. It is a measure of how "thick" or "sticky" a fluid is, and it quantifies the internal friction or resistance between adjacent layers of fluid as they move relative to each other. The concept of viscosity applies to both liquids and gases, although the viscosity of gases is generally lower than that of liquids. The majority of this liquids are optimal and provides some resistance to mobility. This resistance to fluid motion is equivalent to internal friction, which occurs when a solid moves to the surface. The viscosity of a liquid is one of its distinguishing characteristics. When the same velocity is applied to the liquids, but one liquid is more difficult to move than the other, that liquid is said to be more viscous. Liquids that flow quickly have lower resistance, indicating that they are less viscous, whereas liquids that flow slowly and exhibit greater resistance are more viscous, indicating that they have higher viscosity. A fluid with a low viscosity, on the other hand, may flow freely because its molecular forces cause relatively little friction when it is in motion.

3.5.1 Dynamic Viscosity

Dynamic viscosity [124] often denoted by the symbol "μ" (mu), is a fundamental property of fluids that quantifies their resistance to flow under an applied shear stress. It is a measure of the internal friction within a fluid as adjacent layers slide past each other during flow. Dynamic viscosity applies to both liquids and gases, and it plays a crucial role in fluid dynamics, particularly in describing fluid behavior in laminar flow conditions.

$$\text{Viscosity}(\mu) = \frac{\text{Shear stress}}{\text{Velocity gradient}}. \tag{3.4}$$

The SI unit for dynamic viscosity is Ns/m^2 or $kg/m.s$ and its dimension is $\left[\frac{M}{LT}\right]$.

3.5.2 Kinematic Viscosity

Kinematic viscosity [124] often denoted by the symbol "ν" (nu), is a fluid property that relates to the fluid's ability to flow and its resistance to shear under the influence of an applied force. Unlike dynamic viscosity (μ), which quantifies the internal friction within a fluid, kinematic viscosity considers the relationship between dynamic viscosity and fluid density (ρ).

$$\nu = \frac{\mu}{\rho}. \tag{3.5}$$

The SI unit of kinematic viscosity is m^2/s and the dimension is $\left[\frac{L^2}{T}\right]$.

3.6   Newtonian's law of Viscosity

The velocity differential between two neighboring fluid layers directly relates to the shear stress those layers encounter. The velocity gradient $\frac{du}{dy}$, which denotes the rate of change in velocity with respect to the distance perpendicular to the flow direction, is multiplied by the dynamic viscosity μ to produce the shear stress. In other words, the shear stress is the result of the velocity gradient and dynamic viscosity.

$$\tau_{yx} \propto \frac{du}{dy}, \tag{3.6}$$

$$\tau_{yx} = \mu u_y, \tag{3.7}$$

where μ is the dynamic viscosity, τ_{yx} is the shear stress imposed on the fluid element.

The velocity gradient in the y-direction $\frac{du}{dy}$ shows how quickly velocity changes in relation to the y-coordinate [124].

3.7   Newtonian Fluids

A Newtonian fluid [124] is a particular kind of fluid whose viscosity does not alter or fluctuate in response to shear stress or the rate of deformation over time. In other words, the shear stress and shear rate of these fluids are linearly related, and their viscosity is unaffected by the size of the applied force or the length of the deformation. These fluids' viscosity and shear stress have a linear relationship. Newtonian fluids include water, petrol, mineral oil, alcohol, and others.

3.8   Non-Newtonian Fluids

Non-Newtonian fluids [124] are those that exhibit variable viscosity when shear forces are applied. The viscosity of these fluids varies according to the shear force applied, and the connection between shear stress and shear rate is not constant. Non-Newtonian fluids behave differently from Newtonian fluids with constant viscosity because their viscosity can change with increasing shear stress. These are always diametrically opposed to Newtonian fluids. Non-Newtonian fluids include ketchup, liquid cosmetics, toothpaste, wall paint, and so on.

$$\tau_{yx} \propto \left(\frac{du}{dy}\right)^{n}, n \neq 1, \tag{3.8}$$

$$\tau_{yx} = \eta \frac{du}{dy}, \eta = k \left(\frac{du}{dy}\right)^{n-1}, \tag{3.9}$$

where η indicates apparent viscosity, n is the flow behavior index and k is the consistency index.

3.9   Fluid Flow

Numerous characteristics related to a fluid's flow show a variety of modifications when it passes through a certain region or channel. The velocity of the fluid particles and the fluid under consideration are two frequent parameters in the fluid flow. The variables are important

to the fluid motion's dynamics. By examining how flow parameters change over time and space, liquid flow patterns can be categorized. Understanding the fluid motion's dynamic behaviour and how it changes along the way can be made easier with the aid of this classification [124].

3.10   Types of Flow

3.10.1 Steady Flow

The characteristics of a steady flow [124] remain constant as we move from one point in the fluid to another, including velocity and pressure. These conditions don't alter over time and are always the same. In real-world circumstances, flows with absolutely consistent properties throughout time are extremely rare. A steady flow is demonstrated by a fluid flowing through a tapering pipe.

3.10.2 Unsteady Flow

In contrast to steady flow, turbulent flow describes the motion of a fluid where its parameters, like pressure and flow rate change over time at a specific region within the fluid. In other words, the flow is dynamic rather than continuous since its qualities change over time. For example: The movement of flood waves is erratic or unsteady [124].

3.10.3 Uniform Flow

A fluid flow is considered uniform when a flow parameter remains constant as we move along the flow path. Additionally, for a flow to be uniform, the cross-sectional area of the flow must remain consistent. In simpler terms, uniform flow means that the fluid properties, such as velocity or pressure, do not change as we travel along the flow direction. Moreover, the shape and size of the flow's cross-section must remain constant along the flow path. This

concept is crucial in fluid mechanics and engineering, as uniform flow simplifies the analysis of fluid behavior in various applications, such as open-channel flow in rivers and pipes. However, it is important to note that achieving perfect uniform flow is challenging in real-world situations due to various factors such as friction, turbulence and external disturbances. In practice, many flows exhibit slight variations, and understanding these deviations is essential for accurate engineering and design [124].

3.10.4 Non Uniform Flow

Non-uniform flow [124] in contrast to uniform flow refers to fluid motion where the flow parameters change with distance along the flow route. In other words, the fluid properties, such as velocity, pressure or cross-sectional area, vary along the flow direction. In non-uniform flow, the fluid may experience acceleration or deceleration, resulting in changing flow velocities at different points in the flow path. The cross-sectional area of the flow may also vary, leading to fluctuations in flow rate and pressure. This type of flow is common in many practical scenarios, such as flows through curved pipes, around obstacles or in natural waterways with varying topography. Non-uniform flows require more complex analysis compared to uniform flows. The understanding of non-uniform flow is crucial in engineering and fluid dynamics, as it influences the performance and design of various systems, including pipelines, channels and hydraulic structures. Engineers and scientists use mathematical models and computational simulations to study and predict the behavior of non-uniform flows in practical applications.

3.10.5 One dimensional Flow

One-dimensional flow [124] refers to fluid motion where the variations of flow properties (such as velocity, pressure, depth, etc.) occur only in the direction of flow and not across the transverse dimensions of the flow. In other words, the flow properties change along a single axis, which is typically the direction of the flow path. In a one-dimensional flow, all fluid particles move in the same direction with approximately the same velocity and experience similar flow conditions along the flow path. This simplifies the analysis of the flow behavior

because the flow properties can be described using one independent variable, which is usually the distance or time along the flow direction. The one-dimensional flow is commonly observed in systems such as long, straight pipes or channels, open-channel flows with negligible lateral variations, and flow over flat surfaces. These flows are often assumed to be steady and uniform, which allows for easier mathematical modeling and analysis. It is important to note that while one-dimensional flow provides a simplified representation of certain fluid systems, many real-world flows are more complex and may involve two-dimensional or three-dimensional variations in flow properties. Understanding the flow characteristics and limitations of the one-dimensional flow assumption is essential for accurate modeling and engineering design in fluid mechanics.
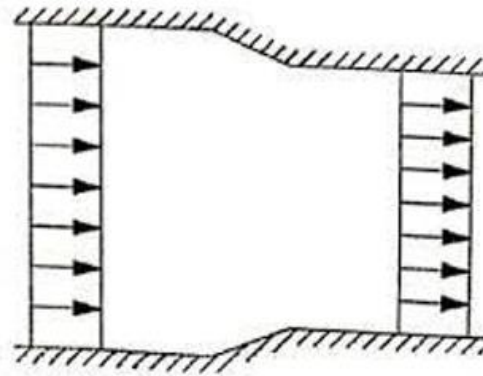
Figure 3.1: One dimensional flow

3.10.6 Two dimensional Flow

Two-dimensional (2D) flow [124] refers to fluid motion in which the variations of flow properties occur in two perpendicular directions, typically represented by the x and y axes of a coordinate system. In other words, the flow properties change in both the longitudinal and transverse directions within the flow domain. In a two-dimensional flow, fluid particles move in various directions with different velocities and experience different flow conditions across the cross-sectional area. This makes the analysis of 2D flows more complex compared to one-dimensional flows. To describe the flow properties in a 2D flow field, two independent variables are typically required. The two-dimensional flow is common in various fluid systems,

including open-channel flows, flow around obstacles, flows in rivers and streams, and some types of pipe flow with significant cross-sectional variations. Understanding 2D flow patterns is crucial in hydraulic engineering, environmental modeling, and other fields that deal with complex fluid behavior.
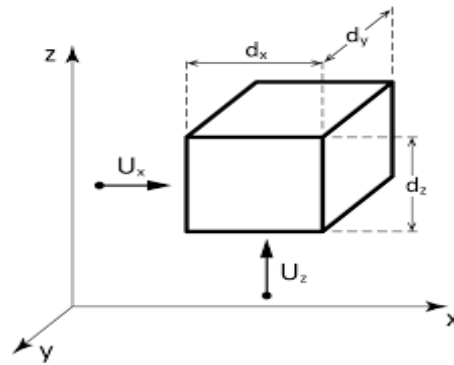
Figure 3.2: Two dimensional flow

3.10.7   Three dimensional Flow

In a three-dimensional liquid's flow, the related parameters vary as function of 3 spatial coordinates and also of time. This means that the flow properties, such as velocity, pressure, temperature, and others, change in all three spatial dimensions (*x, y, z*) and with respect to time (*t*). In 3D flow, the fluid particles move in various directions with different velocities and experience different flow conditions throughout the entire three-dimensional space. The flow field is described by mathematical equations that take into account the variations in flow properties along the three spatial axes and how they evolve over time. This type of flow analysis is more complex than one-dimensional or two-dimensional flow, as it requires solving a system of partial differential equations to fully describe the flow behavior. In many real-world fluid systems, such as turbulent flows, flows around complex geometries, or atmospheric and oceanic flows, considering three-dimensional effects becomes essential for accurate predictions and engineering designs. The understanding of intricacies of three-dimensional fluid flow is crucial in numerous scientific and engineering disciplines, including aerodynamics, hydrodynamics, weather forecasting, and environmental modeling. The accurate simulation and analysis of 3D flow play a vital role in optimizing designs, predicting flow patterns, and evaluating the performance of various fluid systems [124].
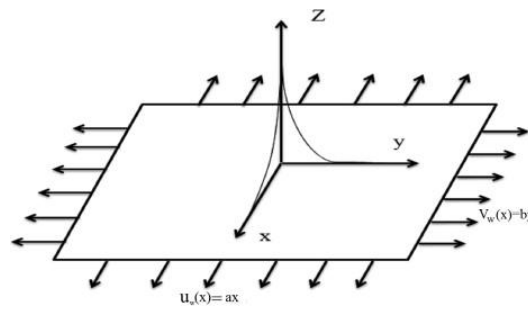
Figure 3.3: Three dimensional flow

3.10.8 Rotational Flow

A fluid particle follows the flow lines while rotating on its own axis in such form of flow. Solid body rotation, the bath tub vortex, laminar flow in a conduit, and wind above the atmospheric boundary layer with minimum shear are all examples of rotational flow [124].

3.10.9 Irrotational Flow

When fluid particles flow along flow lines, they do not spin about their own axis. Irrotational flow [124] is a term used to describe flow that occurs beyond the layer of boundaries. Its examples include flow above a stationary tank's or a wash basin's drain hole.

3.10.10 Laminar Flow

It is categorized as a kind of flow where all streamlines are horizontal and straight and all fluid components move in a specific direction or path. As a result, the particles travel in layers, gently sliding across the nearby layer and also referred to viscous flow. This type of fluid flow is known as Laminar Flow [124].

3.10.11 Turbulent Flow

Fluid particles move randomly and unpredictably in turbulent flow. It is a type of fluid motion characterized by unstable and irregular patterns. Blood flow in arteries, lava flow, oil transit in pipelines, ocean and atmospheric currents flow through turbines and pumps and flow around aircraft-wing tips and in boat wakes are all instances of turbulent flow [124].

3.10.12 Compressible Flow

It is a category of fluid flow where changes in pressure, temperature and velocity significantly affect the fluid's density. As a result, it is impossible to assume that the flow characteristics would remain constant during the entire process and the compressibility of the fluid has a substantial impact on how it behaves. This kind of flow is frequently seen in gases and high-speed fluxes, as those found in rocket engines and supersonic aircraft [124].

3.10.13 Incompressible Flow

When a fluid flows in an incompressible manner, its volume does not considerably vary along the flow path and its density stays essentially constant. The fluid's density changes very little in an incompressible flow [124] which is often seen at slower flow rates and in liquids. The analysis of the flow is made simpler by the assumption of incompressibility, making it simpler to model and determine different parameters including pressure, velocity and flow patterns. When it is possible to ignore density changes, incompressible flow is frequently used to analyze flows in pipelines, water systems, and many other technical applications.

3.11 Mechanism of Heat Flow

There are three different ways for heat to go from one body to another [125].

3.11.1 Conduction

In stationary fluids and solids, conduction is a means of heat transfer. This heat is transferred through direct molecular contact, when more energetic molecules give their energy to nearby molecules with lower energies. This heat transmission in solids happens as a result of atom or molecule collisions and vibrations. Conduction in stationary fluids (liquids and gases) is mostly caused by molecular collisions. There are some examples of conduction [125] process like burning your feet on hot sand, transferring heat from a hob to a saucepan filled with water, burning a marshmallow in a campfire by touching the marshmallow to the flame.

3.11.2 Convection

Convection [125] is a type of heat transmission that takes place in fluids (liquids and gases), where heated fluid particles carry energy with them as they travel away from the heat source. Warmer fluid near a heat source becomes less dense and rises as a result of buoyancy forces. While the fluid rises, cooler fluid from the vicinity flows in to replace it, resulting in a continuous circulation pattern called convection currents. Few examples of convection process include hot air rises above a fire in a plume, melting of ice is occurring, sea breeze or land breeze results from a pressure difference, blood circulation in warm-blooded animals.

3.11.3 Radiation

Radiation [125] involves the transport of temperature by electromagnetic radiation such as visible light, UV, and infrared radiation. Anything above absolute zero emits heat. Some examples of radiation can be expressed by uranium's radioactive decay generates alpha particles or sound waves in a stereo. Likewise microwaves generated by a microwave oven and UV light emitted by a black lamp.

3.12   Thermal Conductivity

Thermal conductivity [124] is a physical property of materials that quantifies their

ability to conduct heat. It is a measure of how efficiently a material can transfer heat through direct molecular interactions. High thermal conductivity indicates that a material can rapidly conduct heat, while low thermal conductivity means that the material is a poor conductor of heat. The materials with high thermal conductivity, such as metals like copper and aluminum, are excellent at transferring heat and are often used in applications where efficient heat conduction is required, such as heat sinks in electronic devices. On the other hand, materials with low thermal conductivity, such as insulators like wood or fiberglass, are used to prevent heat transfer in applications like building insulation.

The thermal conductivity of a material depends on its chemical composition, structure, and temperature. It is usually measured in $W/m \cdot K$ and is an essential parameter in understanding heat transfer processes and designing various thermal systems.

$$\text{Thermal conductivity} = \frac{\text{heat} \times \text{distance}}{\text{area} \times \text{Temperature gradient}}, \tag{3.10}$$

$$k = \frac{QL}{A\Delta T}, \tag{3.11}$$

where Q denotes heat, L represents distance, A is the area and ΔT is temperature gradient.

3.13   Thermal Diffusivity

The rate of heat transmission of a substance or material from the hot side to the cold side is measured by its thermal diffusivity [124] which is calculated by dividing its thermal conductivity with its density and specific heat capacity at constant pressure. It indicates how rapidly a material responds to a change in temperature and is a material-specific feature for describing unstable heat conduction.

$$\alpha^* = \frac{k}{\rho c_p}, \tag{3.12}$$

where ρ is density, k denotes thermal diffusivity and c_p represents specific heat capacity. If the thermal diffusivity is more than the volumetric heat capacity, the rate of heat transmission will be higher.

The SI unit for thermal diffusivity is m^2/s and has dimension $\left[\frac{L^2}{T}\right]$.

3.14   Brownian Motion

Brownian motion [124] describes the random movement of tiny particles floating in fluids. It is usually known as the Brownian movement. This motion is caused by particle collisions with other fast-moving particles in the fluid. The examples can be found in pollen grains moving in motionless water or the movement of dust motes in a room can also be its example.

3.15   Thermophoresis

Thermophoresis [124] is a phenomena found in movable particle mixtures in which various particle respond differently to the force of a temperature difference. This process tends to transfer light molecules to hot regions and heavy ones to cool locations. When the hot rod of an electric heater is surrounded by tobacco smoke, the smoke moves away from the hot rod is an example of thermophoresis.

3.16   The Permeability of a Porous Medium

The ease with which a fluid will flow through a porous medium is known as its permeability. The higher the permeability, the higher the flow rate for a given hydraulic gradient. The fluid conductivities in all the flow channels of the solid body are statistically averaged to produce the permeability [125].

3.17   Dimensionless Numbers

A numerical value that denotes a physical system's attribute, but isn't quantified using physical units [125].

3.17.1 Reynolds Number

The Reynolds number [125] a dimensionless quantity, is defined as the ratio of inertial and viscous forces and can be used to distinguish between these two types of flow patterns. The initial forces rise as the flow velocity increases, as does the Reynolds Number. The Reynolds number is less than 2000 in laminar flow and greater than 2000 in turbulent flow. It is defined as:

$$\text{Re} = \frac{\text{inertial force}}{\text{viscous force}}, \tag{3.13}$$

$$Re = \rho V D / \mu. \tag{3.14}$$

In which ρ is the density, V is the velocity of flow, D is the pipe diameter, μ is dynamic viscosity.

3.17.2   Prandtl Number

A dimensionless number called the Prandtl number [125] connects a fluid's viscosity to its thermal conductivity. As a result, it evaluates the relationship between momentum transfer and a fluid's capability for heat transport.

It is defined as:

$$\text{Pr} = \frac{\text{Momentum transport}}{\text{Heat transport}}, \tag{3.15}$$

$$Pr = \frac{\nu}{\alpha^*} = \frac{\mu c_p}{k}, \tag{3.16}$$

where ν is the kinematic viscosity, α^* is thermal diffusivity, μ is the dynamic viscosity and c_p is specific heat. If Pr $\ll$ 1, then thermal diffusivity take over and if Pr $\gg$ 1 , then momentum diffusivity controls. Small Prandtl values are a suitable choice for heat transmitting liquids since they are free-flowing liquids with strong thermal conductivity.

3.17.3 Lewis Number

Lewis number [125] denoted as *Le*, denotes the correlation between heat diffusivity and also mass diffusivity and is demanded in thermodynamics and fluid. It has not at all any dimensions. It is frequently used to describe scenarios of fluid flow that involve both heat and mass transport. Calculating the Lewis number involves dividing heat diffusivity by mass diffusivity.

$$Le = \frac{\alpha}{D} = \frac{\lambda}{\rho\, D_{im} c_p}, \tag{3.17}$$

where c_p is the specific heat, α is symbolized for thermal diffusivity, λ is noted for thermal conductivity, D_{im} is denoted for mixture averaged diffusion coefficient and D is symbolized for mass diffusivity.

3.17.4 Sherwood Number

A dimensionless and important parameter used in mass transferal operations is noted as Sherwood number (Sh) [125] also referred to as the mass transfer Nusselt number. It denotes the interaction between rate of diffusive mass transport and convective mass transferal. In contrast to the slower diffusion-driven mass transport, it measures the effectiveness of mass transfer caused by fluid motion.

$$Sh = \frac{\text{Convective mass transfer rate}}{\text{Diffusion rate}} = \frac{hL}{D}, \tag{3.18}$$

where h is the convective mass transfer film coefficient, L a characteristic length, D is the mass diffusivity.

3.17.5 Nusselt Number

The amount of convective heat transmission vs conductive heat transfer across a barrier is contrasted using the Nusselt number [125] a dimensionless metric. It can be stated mathematically as follows:

$$\text{Nu}_{\text{L}} = \frac{\text{Convection heat transfer}}{\text{Conductive heat transfer}}. \tag{3.19}$$

The Newton's law of cooling gives

$$q' = h\Delta T, \tag{3.20}$$

where h signifies coefficient of heat transfer and q' signifies the flux per unit area.

Heat flow for the convectional process is

$$q' = h(T_w - T_\infty). \tag{3.21}$$

Additionally, if the fluid layer remains static, the heat influx for the process of conduction is provided by

$$q' = \frac{k(T_w - T_\infty)}{L}, \tag{3.22}$$

where k signifies fluid's thermal conductivity and L signifies the characteristic length.

From the definition of Nusselt number, we get

$$Nu_L = \frac{h(T_w - T_\infty)}{k(T_w - T_\infty)} = \frac{hL}{k}. \tag{3.23}$$

3.17.6 Skin Friction

Hydrodynamic drag, which is a restraining force applied to an object moving in a fluid, involves skin friction drag. The skin friction coefficient can be expressed mathematically as

$$C_f = \frac{\tau_w}{\left(\frac{1}{2}\right)\rho U^2} \tag{3.24}$$

where τ_w is shear stress for wall, U represents velocity and ρ denotes density [125].

CHAPTER 4

THE HEAT AND MASS TRANSFER ANALYSIS FOR MAGNETOHYDRODYNAMIC FLOW OF PRANDTL-EYRING NANOFLUID PAST A STRETCHABLE SURFACE

4.1   Introduction

The flow of a two-dimensional Prandtl Eyring nanofluid across a stretched surface is investigated. The fluid is assumed to be incompressible. The heat and mass transfer analysis has been explored. The system is presented as complicated partial differential equations. Appropriate similarity transformations result in the reduction of the controlling these differential equations to simplified differential equations which are nonlinear equations. In order to solve these ordinary differential equations (nonlinear), the BVP4c technique is used. The consequences of associated factors are visually depicted. The local Nusselt number, skin friction coefficient and Sherwood number are all numerically calculated. A comparison with prior work is carried out to confirm the accuracy of the current results. This chapter provides a comprehensive assessment of the study article authored by Abdelmalek *et al.* [126].
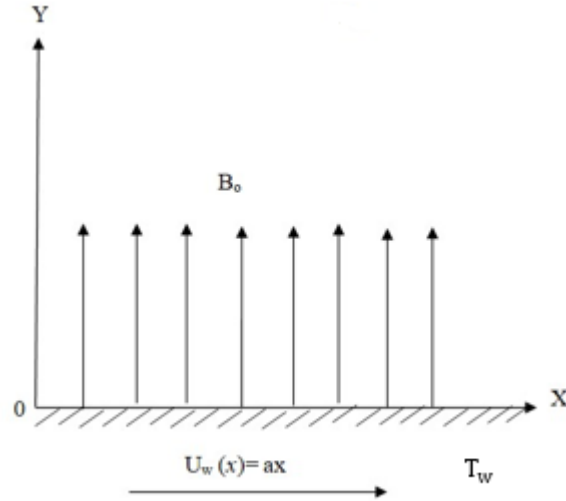
Figure 4.1: Geometry of the problem

4.2 Mathematical Formulation

A steady and magnetohydrodynamic (MHD) flow for a non-Newtonian fluid across a stretched surface is taken. The surface is stretching with a linear velocity and external magnetic field having a strength B_0 is applied. The Cartesian coordinate system is taken for this two dimensional flow. The boundary layer flow velocity field is given by:

$$\mathbf{V} = [u(x,y), v(x,y), 0]. \tag{4.1}$$

The general form of the continuity, momentum, energy and concentration equations are as follows Abdelmalek *et al.* [126].

$$\nabla . \mathbf{V} = \mathbf{0}, \tag{4.2}$$

$$\rho \frac{d\mathbf{V}}{dt} = \nabla . \mathbf{T} + \mathbf{J} \times \mathbf{B}, \tag{4.3}$$

$$(\mathbf{V}.\nabla)T = \alpha_f \, \nabla^2 T + \tau \left[D_B \nabla C. \nabla T + \frac{D_T}{T_\infty} \nabla T. \nabla T \right], \tag{4.4}$$

$$(\mathbf{V}.\nabla)C = D_B \nabla^2 C + D_T \frac{\nabla^2 T}{T_\infty}. \tag{4.5}$$

Where ρ is noted for density, **V** for velocity field, **J** for electric current density, **B** for magnetic field, $\frac{d}{dt}$ for material time, **T** for Cauchy stress tensor, α_f for thermal diffusivity, τ for the ratio of heat capacity of nanoparticle and base fluid, D_B and D_T for the Brownian and thermophoretic diffusion coefficients, T_∞ for the ambient temperature of the fluid.

The stress tensor for the flow can be stated as

$$\mathbf{T} = -p\mathbf{I} + \mu\mathbf{S},\tag{4.6}$$

where

$$\mathbf{S} = \frac{\text{Asinh}^{-1}\left(\frac{1}{c}\sqrt{\frac{1}{2}\text{tr}(A_1^2)}\right)}{\sqrt{\frac{1}{2}\text{tr}(A_1^2)}}A_1.\tag{4.7}$$

In the above equations, S is extra stress tensor for the considered fluid, p is pressure, μ is dynamic viscosity, A_1 is first Rivilin-Erickson tensor, A and C are parameters for non-Newtonian fluid.

Under the considered assumptions, the governing Eqs. (4.2) - (4.5) reduce to the following forms

$$\frac{\partial u}{\partial x} + \frac{\partial v}{\partial y} = 0,\tag{4.8}$$

$$u\frac{\partial u}{\partial x} + v\frac{\partial u}{\partial y} = \frac{A}{\rho c}\frac{\partial^2 u}{\partial y^2} - \frac{A}{2\rho c^3}\left(\frac{\partial u}{\partial y}\right)^2\frac{\partial^2 u}{\partial y^2} - \frac{\sigma B_0^2}{\rho}u,\tag{4.9}$$

$$u\frac{\partial T}{\partial x} + v\frac{\partial T}{\partial y} = \alpha\frac{\partial^2 T}{\partial y^2} + \tau D_B\left(\frac{\partial T}{\partial y}\frac{\partial C}{\partial y}\right) + \frac{\tau D_T}{T_\infty}\left(\frac{\partial T}{\partial y}\right)^2,\tag{4.10}$$

$$u\frac{\partial C}{\partial x} + v\frac{\partial C}{\partial y} = D_B\frac{\partial^2 C}{\partial y^2} + \frac{D_T}{T_\infty}\frac{\partial^2 T}{\partial y^2}.\tag{4.11}$$

With associated boundary conditions mentioned as

$$u = U_w(x) = ax, v = 0, T = T_w, C = C_w \quad \text{at } y = 0,$$

$$u \rightarrow 0, T \rightarrow T_\infty, C \rightarrow C_\infty \text{ at } y \rightarrow \infty.\tag{4.12}$$

The steam flow function is represented as:

$$u = \frac{\partial \psi}{\partial y}, \quad v = -\frac{\partial \psi}{\partial x}.\tag{4.13}$$

Setting the following transformations

$$\eta = y\sqrt{\frac{a}{\upsilon}}, \quad \psi = \sqrt{a\upsilon}\, xf(\eta), \quad \theta = \frac{T-T_\infty}{T_w-T_\infty}, \quad \varphi = \frac{C-C_\infty}{C_w-C_\infty}.\tag{4.14}$$

Appling the similarity transformation on questions Eqs. (4.8) – (4.12) the following equations are obtained

$$\alpha f''' - \alpha \beta f''^2 f''' - f'^2 + ff'' - Mf' = 0, \tag{4.15}$$

$$\theta'' + \Pr[f\theta' + Nb\theta'\varphi' + Nt(\theta')^2] = 0, \tag{4.16}$$

$$\varphi'' + Le\Pr f\varphi' \frac{Nt}{Nb}\theta'' = 0. \tag{4.17}$$

$$f = 0, f' = 1, \theta = 1, \varphi = 1 \; at \; \eta = 0.$$
$$f' \to 0, \theta \to 0, \varphi \to 0 \; at \; \eta \to \infty. \tag{4.18}$$

The dimensionless parameters are mentioned as:

$$Le = \frac{\alpha}{D_B}, \beta = \frac{\alpha^3 x^2}{2c^2 \upsilon}, \; M = \frac{\sigma B_0^2}{\alpha \rho}, \alpha = \frac{A}{\mu c}, \tag{4.19}$$

$$Nt = \frac{\tau D_T (T_w - T_\infty)}{T_\infty \upsilon}, \; Nb = \frac{\tau D_B (C_w - C_\infty)}{\upsilon}, \; \Pr = \frac{\upsilon}{\alpha 1},$$

in which *Le* denotes Lewis number, α and β represents non-dimensional fluid parameters, *M* is the Hartmann number, Pr is the Prandtl number, N_t is the thermoporesis parameter, N_b represents Brownian motion parameter.

The coefficient of skin friction C_f, the local Nusselt number Nu_x and Sherwood number Sh_x are defined as follows

$$C_{fx} = \frac{\tau_w}{\frac{1}{2}\rho U^2}, \quad Nu_x = \frac{xq_w}{k(T_w - T_\infty)}, Sh_x = \frac{xq_m}{D_B(C_w - C_\infty)}, \tag{4.20}$$

with

$$\tau_w = \frac{A}{C}\left(\frac{\partial u}{\partial y}\right)_{y=0} - \frac{A}{6C^3}\left(\frac{\partial u}{\partial y}\right)^2_{y=0}, \; q_w = -k\left(\frac{\partial T}{\partial y}\right)_{y=0}, \; q_m = D_B\left(\frac{\partial C}{\partial y}\right)_{y=0}. \tag{4.21}$$

Putting values of τ_w, q_w and q_m in Eq. (4.20),

$$\frac{1}{2}Cf_x Re_x^{\frac{1}{2}} = \alpha f''(0) - \frac{\alpha\beta}{3}[f''(0)]^3, \; Nu_x Re_x^{-\frac{1}{2}} = -\theta'(0), \tag{4.22}$$

$$Sh_x Re_x^{-\frac{1}{2}} = -\varphi'(0).$$

4.3   Numerical Stratagem

To solve the governed flow ODEs equations, the MATLAB tool bvp4c is applied. In general, the derived equations are higher order differential equations. In the first phase, these differential equations are reduced to first order form, and these first order differential equations are solved out using bvp4c method.

$$f_1 = f, \tag{4.23}$$

$$f_2 = f_1' = f', \tag{4.24}$$

$$f_3 = f_2' = f'', \tag{4.25}$$

$$f_5 = \theta, \tag{4.26}$$

$$f_6 = f_5' = \theta', \tag{4.27}$$

$$f_8 = \varphi, \tag{4.28}$$

$$f_9 = f_8' = \varphi'. \tag{4.29}$$

Eqs. (4.15) - (4.17) can be written as:

$$f_4 = f_3' = f''' = \frac{(f_2)^2 + f_1 f_3 - M f_2}{\alpha - \alpha\beta(f_3)^2}, \tag{4.30}$$

$$f_7 = f_6' = \theta'' = -Pr(f_1 f_6 + Nb f_6 f_9 + Nt(f_6)^2), \tag{4.31}$$

$$f_{10} = f_9' = \varphi'' = -\frac{Nt}{Nb} f_7 - PrLe f_1 f_9. \tag{4.32}$$

4.4   Graphical Analysis and Discussion

In this section, the prominent effects of several parameters on velocity, temperature and also concentration profiles are explored graphically and also the variation in skin friction coefficient, Nusselt number and Sherwood number with respect to the parameters are a part of the study. Figure 4.2 illustrates the impact of Prandtl Eyring fluid

parameter α on velocity profile. Increase in α cause proliferation in velocity profile $f'(\eta)$. Prandtl Eyring fluid parameter rushes the fluid flow momentum within the boundary layer domain, moreover, if $\alpha > 1$, a significant increase in is seen relative to the velocity. The viscous forces are diminished for higher levels of the relevant parameter. Figure 4.3 depicts the fluctuations in fluid velocity of Prandtl Eyring fluid parameter β and it is seen that increase in β cause diminution in velocity profile $f'(\eta)$. Small values of fluid parameter β demonstrate significant slowdown in linear momentum and thickness of boundary layer. Fig 4.4 signifies the impact of Hartmann number M on velocity profile $f'(\eta)$. The increase in Hartmaan number M respond to fading velocity profile $f'(\eta)$. The effect of thermophoresis parameter Nt on temperature profile $\theta'(\eta)$ is portrayed in Figure 4.5. It is observed that increase in thermophoresis parameter Nt cause increase in temperature profile $\theta'(\eta)$. The thermophoresis phenomenon quickens particles movement from hotter to cooler regions, and heat transfer occurs as a result. A rapid heat transfer is observed from a heated surface to a fluid, raising the temperature. The current result confirms the above mentioned hypothesis. Figure 4.6 illustrates the deviation of Brownian motion parameter Nb for temperature profiles $\theta'(\eta)$. It is monitored that surge in Brownian motion parameter Nb can increase the temperature profile $\theta'(\eta)$. Figure 4.7 depicts the variant Prandtl number Pr on temperature profile $\theta'(\eta)$. The higher Prandtl number Pr leads to a decrease for temperature profile $\theta'(\eta)$. The relationship among thermal conductivity and viscous conductivity is described through Prandtl number Pr, thus a fluid with an advanced Prandtl number possesses lower thermal conductivity. The figure designates a drop in temperature affectedly in the boundary layer regime with raised Prandtl number. Figure 4.8 denotes the effects of Brownian motion Nb on nanoparticle concentration profile $\varphi'(\eta)$ and the image indicates that Brownian motion Nb shrinkages both concentration profile $\varphi'(\eta)$ as well ad the solutal boundary layer thickness. As increase of Brownian motion Nb sources the haphazard movement to quickens, dispersing the nanoparticles and tumbling concentration profile $\varphi'(\eta)$. The variation of thermophoresis parameter Nt is noticed for concentration profile $\varphi'(\eta)$ in Figure 4.9. It can be seen as in the figure that concentration profile $\varphi'(\eta)$ develops swiftly when thermophoresis parameter Nt is augmented within the flow domain. Figure 4.10 expresses the impact of Lewis number Le on the concentration profile $\varphi'(\eta)$. The upsurge in Lewis number Le weakens the concentration profile $\varphi'(\eta)$. The Lewis number Le, known to be the ratio of thermal to mass diffusivity, thus advanced values of Lewis number Le shrink mass diffusivity

resulting in less concentration profile $\varphi'(\eta)$. Figure 4.11 clarifies the variations in concentration profile $\varphi'(\eta)$ caused by changing Prandtl number Pr. This graph predicts that Pr significantly reduces nanoparticle concentration profile $\varphi'(\eta)$. Furthermore, when Prandtl number Pr is large, the solutal boundary layer is insignificant.

Table 4.1 indicates that the result of varying different parameters for the wall friction and it boosts when the Prandtl Eyring fluid parameter α and Hartmann number H grows, while the Prandtl Eyring fluid parameter β drops down the wall friction. Table 4.2 represents the wall heat flux interms of dimensionless parameters. The heat transfer is accelerated against the Prandtl number Pr, whereas thermophoresis parameter Nt and Brownian motion parameter Nb offer resistance to heat transfer from the surface. Table 4.3 shows that the significant parameters Prandtl number Pr, Lewis number Le and Brownian motion parameter Nb intensify the wall mass flux while thermophoresis parameter Nt condenses the mass flux.
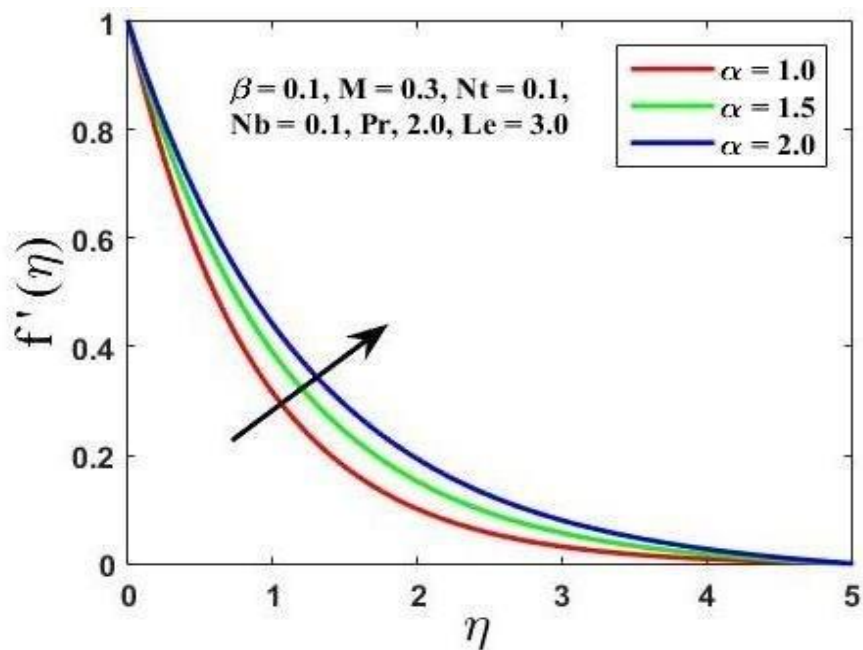
Fig 4.2: Velocity sketch in case of variability in α.
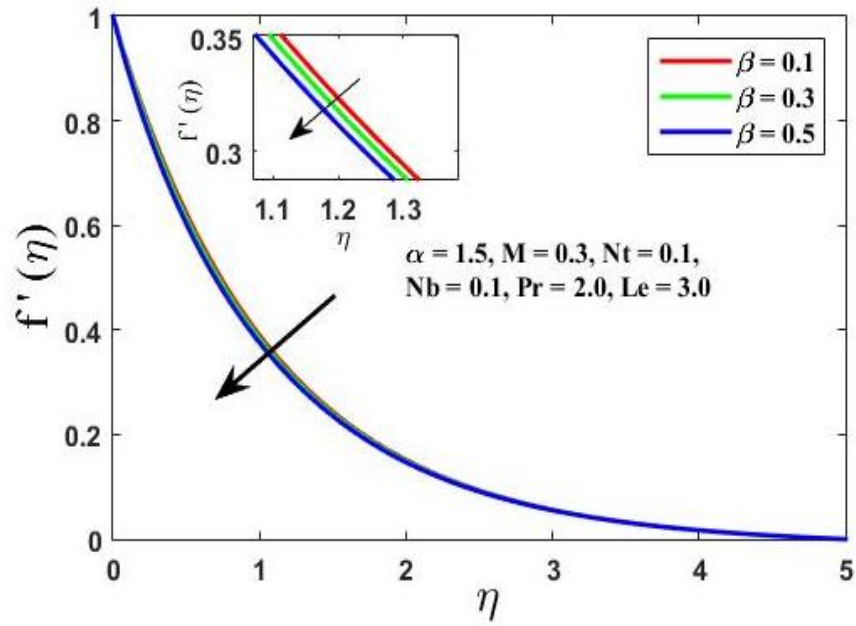
Fig 4.3: Velocity sketch in case of variability in β.
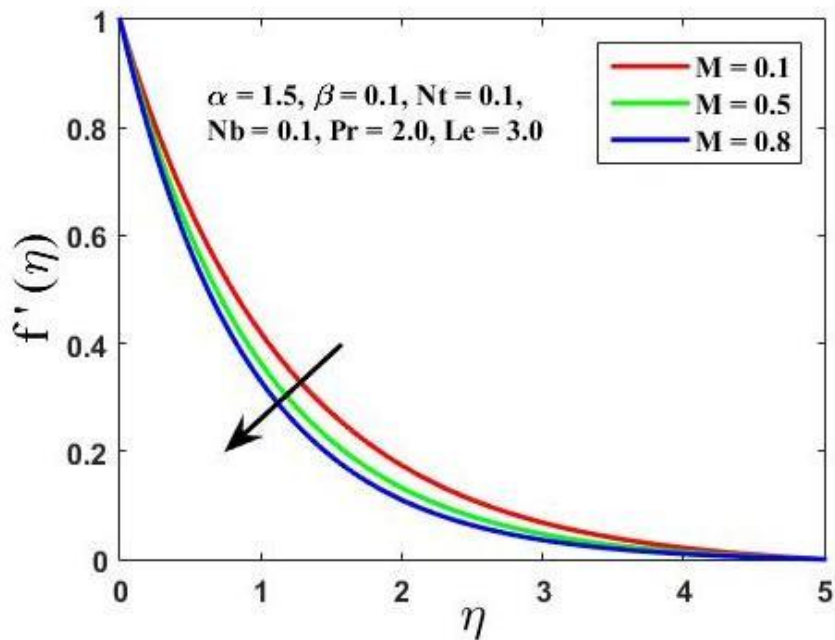
Fig 4.4: Velocity sketch in case of variability in M.
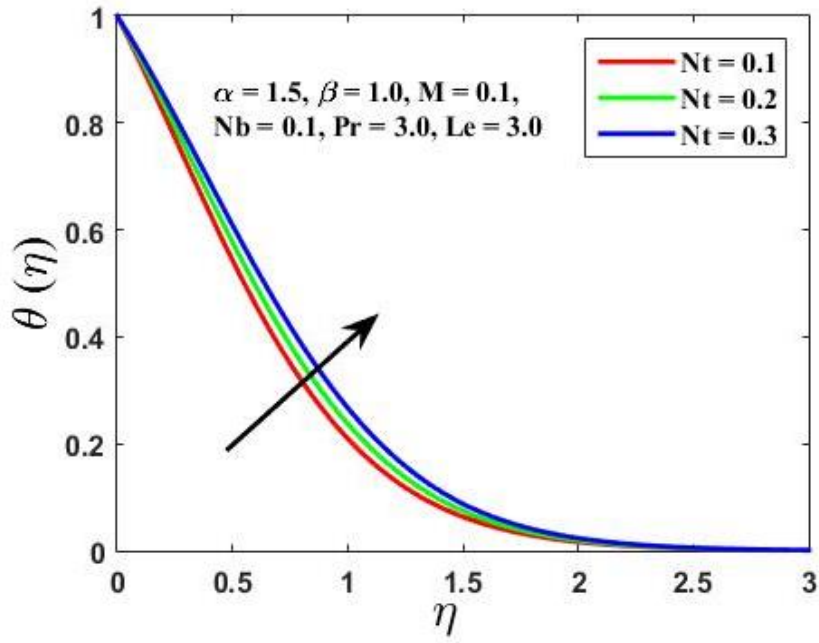
Fig 4.5: Temperature sketch in case of variability in *Nt*.
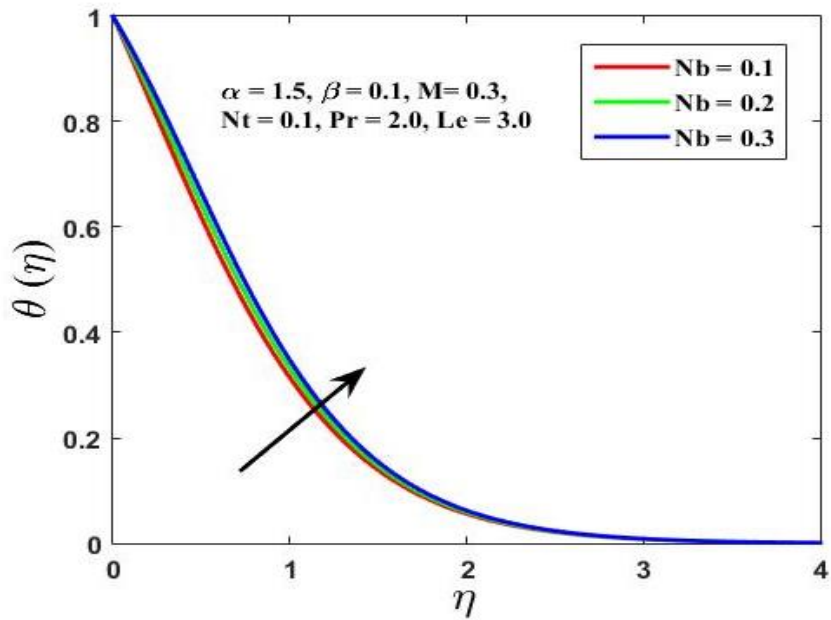
Fig 4.6: Temperature sketch in case of variability in *Nb*.
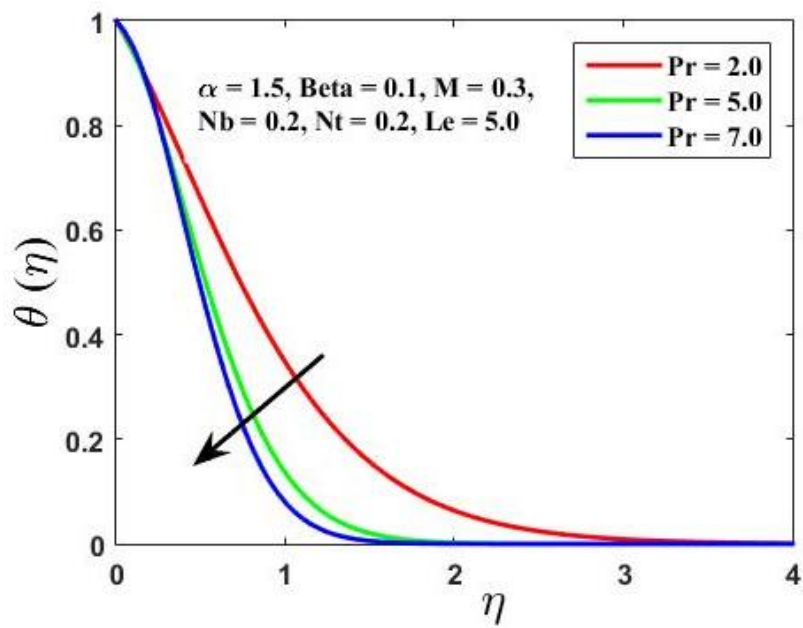
Fig 4.7: Temperature sketch in case of variability in Pr.
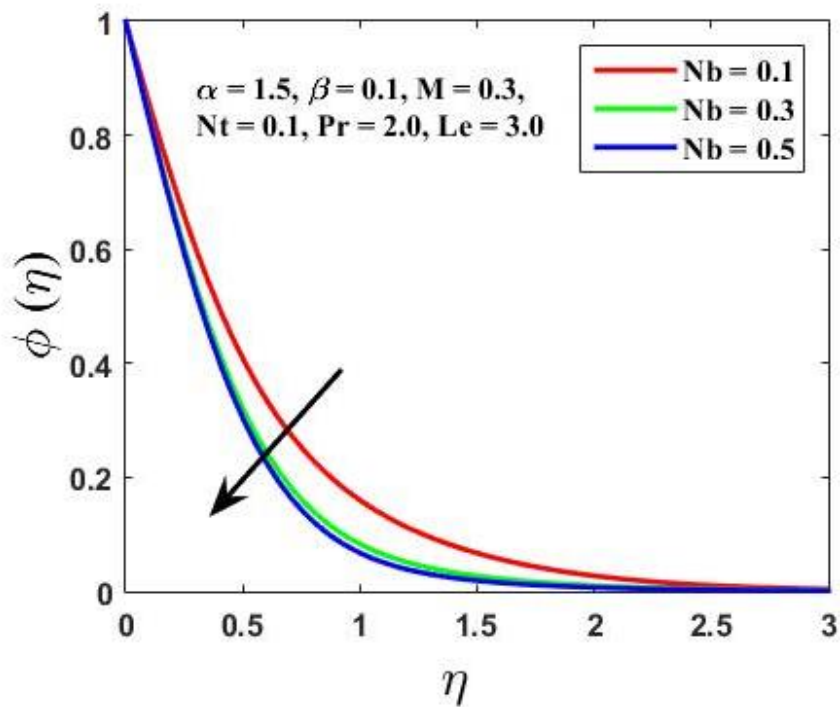
Fig 4.8: Concentration sketch in case of variability in *Nb*.
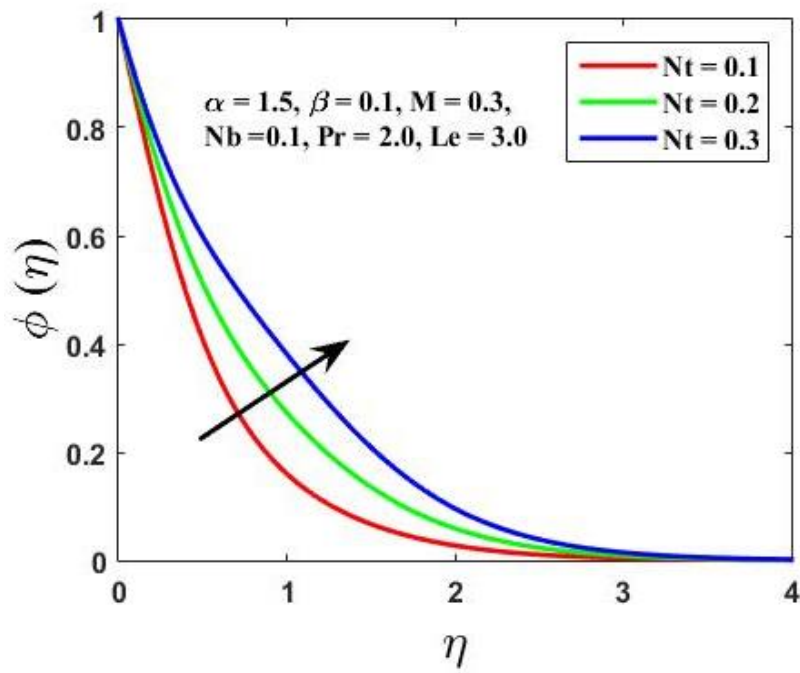
Fig 4.9: Concentration sketch in case of variability in *Nt.*
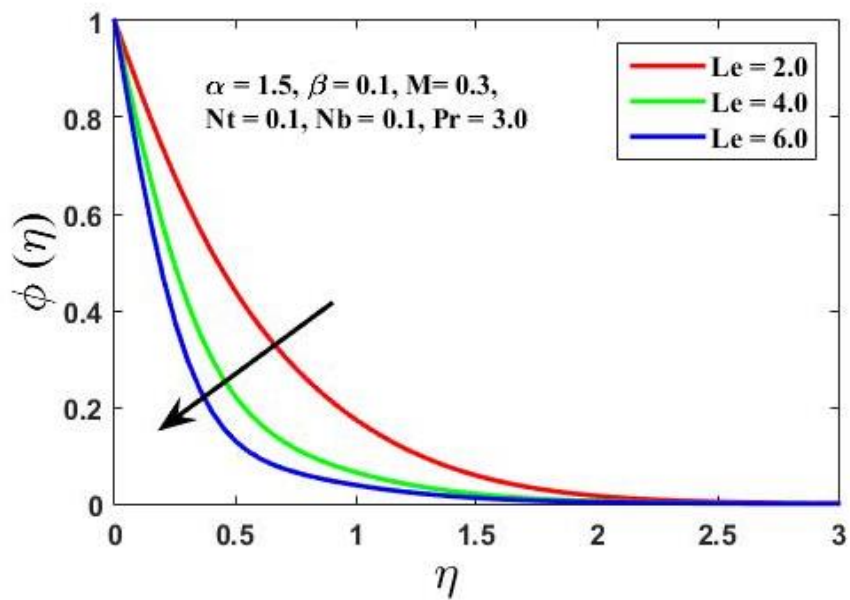
Fig 4.10: Concentration sketch in case of variability in *Le.*
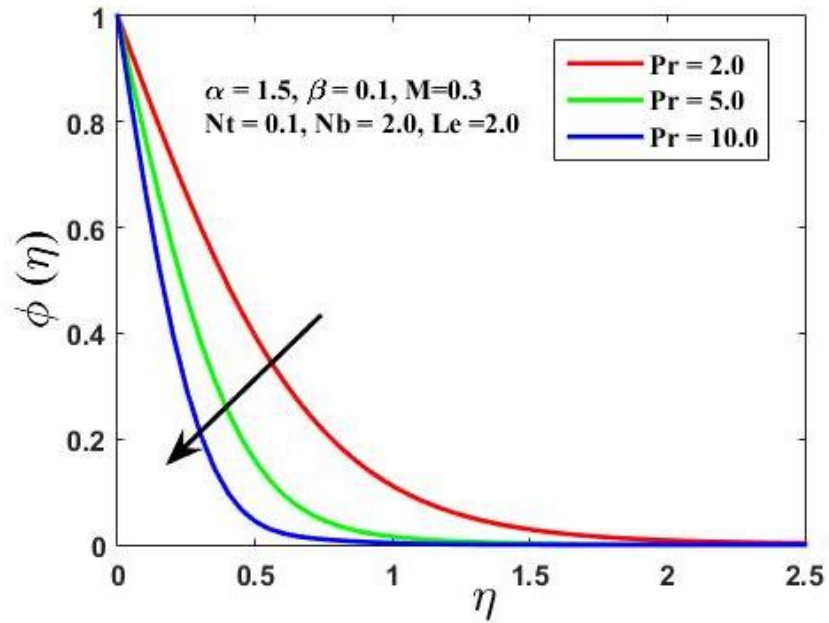
Fig 4.11: Concentration sketch in case of variability in Pr.

Table 4.1: Comparative values of skin friction coefficient for *M* if $\alpha = 1,\ \beta = 0$.

M	Fatehzadeh *et al.* [127]	Akbar *et al.* [128]	Abdelmalek *et al.* [126]	Present Results
0	-1	-1	-1.004	-1.0014
0.5	-	-1.11803	-1.1180	-1.1181
1.0	-1.41412	-1.41421	-1.4140	-1.4142
5.0	-2.44948	-2.44949	-2.4494	-2.4495
10	-3.31662	-3.31663	-3.3168	-3.3166
50	-7.14142	-	-4.4143	-7.1414
100	-10.0499	-10.04889	-10.0502	-10.0499
500	-22.383	-22.38303	-22.3831	-22.3830
1000	-31.6368	-31.63859	-31.6387	-31.6386

Table 4.2: Variation in skin friction coefficient by changing of physical parameters α, β and M when Pr = 2.0, Le = 3.0, Nb = 0.1, Nt = 0.1.

α	β	M	Skin friction coefficient
1.0	0.1	0.3	1.1259
1.5			1.3863
2.0			1.6067
3.0			1.9815
1.5	0.1		1.3863
	0.2		1.3736
	0.3		1.3597
	0.4		1.3442
	0.1	0.1	1.2785
	0.1	0.3	1.3863
		0.5	1.4865
		0.8	1.6247

Table 4.3: Variation in Nusselt number $(-\theta'(0))$ by changing physical parameters Pr, Nb, Nt when α = 1.5, β = 0.1, M = 0.3, Le = 3.0.

Pr	Nb	Nt	Nusselt number
2.0	0.1	0.1	0.7406
5.0			0.9060
7.0			1.1717
2.0	0.1		0.7406
	0.2		0.6415
	0.3		0.5538
	0.5		0.4089
	0.1	0.1	0.7406
		0.2	0.6840
		0.3	0.6328
		0.4	0.5866

Table 4.4: Variation in Sherwood number $(-\varphi'(0))$ by changing physical parameters Pr, *Nb, Nt* and *Le* when $\alpha = 1.5$, $\beta = 0.1$ and $M = 0.3$.

Pr	Nb	Nt	Le	Sherwood number
2.0	0.1	0.1	3.0	1.4725
5.0				2.7226
7.0				3.4189
10.0				4.3321
2.0	0.1			1.4725
	0.2			1.6490
	0.3			1.7045
	0.5			1.7436
	0.1	0.1		1.4725
		0.2		1.2679
		0.3		1.1229
		0.4		1.0259
		0.1	3.0	1.4725
			5.0	2.1086
			7.0	2.6104
			10.0	3.2309

CHAPTER 5

IMPACT OF INCLINED MAGNETIC FIELD ON STAGNATION POINT FLOW OF NANOFLUID OVER A STRETCHING SHEET

5.1 Introduction

A two dimensional and laminar flow of Prandtl-Eyring nanofluid flowing due to stretching surface placed in a porous medium is investigated in the chapter. The nanofluidic flow model is constructed with the occurrence of stagnation point and an inclined magnetic field. The assumed problem is depicted through a complicated set of differential equations. By means of transformation, the concentration equation, energy equation and momentum equation are transmuted as ordinary equations, which are later solved utilizing the bvp4c approach. The results are graphically examined and the influence of significant parameters on concentration distribution, temperature distribution and velocity distribution is revealed. The coefficient of skin friction (Cf_x), local Nusselt number (Nu_x) and sheward number (Sh_x), are calculated and examined numerically.
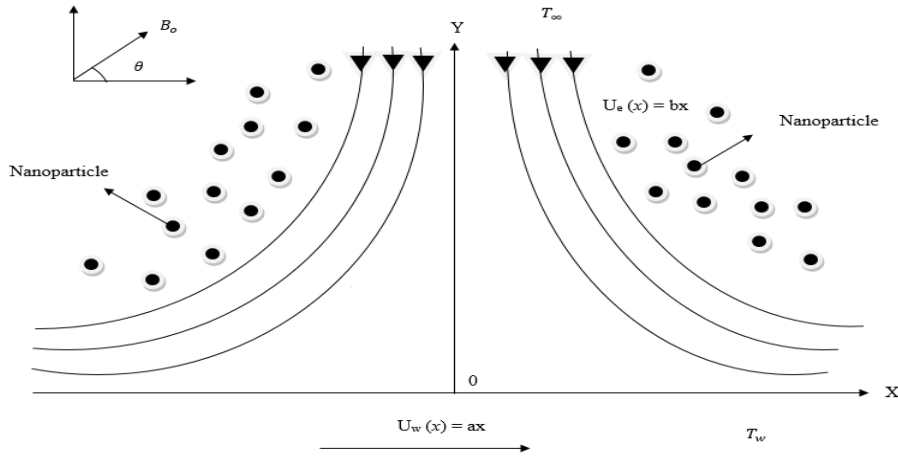
Figure 5.1: Geometry of the problem.

5.2   Mathematical Model

The steady and two-dimensional flow of Prandtl-Eyring nanofluid across a stretching surface is investigated. The surface is stretching in the *x*-direction with linear velocity $U_w(x) = ax$. The experiment is carried out in the presence of a stagnation point, and the considered flow is further subjected to an inclined magnetic field. For the given flow, the Buon-giorno nano-model is employed to examine mass and also heat transfer with the effects of thermophoretic forces and Brownian motion on the flow.

$$\mathbf{V} = [u(x, y), v(x, y), 0], \tag{5.1}$$

The general form of the continuity, momentum, energy and concentration equations are as follows Abdelmalek *et al.* [126].

$$\boldsymbol{\nabla} . \mathbf{V} = \mathbf{0}, \tag{5.2}$$

$$\rho \frac{d\mathbf{V}}{dt} = \boldsymbol{\nabla} . \mathbf{T} + \mathbf{J} \times \mathbf{B}, \tag{5.3}$$

$$(\mathbf{V}.\boldsymbol{\nabla})T = \alpha_f \boldsymbol{\nabla}^2 T + \tau \left[D_B \boldsymbol{\nabla} C . \boldsymbol{\nabla} T + \frac{D_T}{T_\infty} \boldsymbol{\nabla} T . \boldsymbol{\nabla} T \right], \tag{5.4}$$

$$(\mathbf{V}.\boldsymbol{\nabla})C = D_B \boldsymbol{\nabla}^2 C + D_T \frac{\boldsymbol{\nabla}^2 T}{T_\infty}. \tag{5.5}$$

Where ρ is signified by density, **V** by velocity field, **J** by electric current density, **B** by magnetic field, $\frac{d}{dt}$ by material time, **T** by Cauchy stress tensor, α_f by thermal diffusivity, τ by the ratio of heat capacity of nanoparticle and base fluid, D_B and D_T by the Brownian and thermophoretic diffusion coefficients, T_∞ by the ambient temperature of the fluid.

The stress tensor for the considered non-Newtonian fluid is given by:

$$\mathbf{T} = -p\mathbf{I} + \mu\mathbf{S}, \tag{5.6}$$

where
$$\mathbf{S} = \frac{\text{Asinh}^{-1}\left(\frac{1}{c}\sqrt{\frac{1}{2}\text{tr}(A_1^2)}\right)}{\sqrt{\frac{1}{2}\text{tr}(A_1^2)}}A_1. \tag{5.7}$$

It is to be noted that S is extra stress tensor for the considered fluid, p is pressure, μ is dynamic viscosity, A_1 is first Rivilin-Erickson tensor, A and C are parameters for Prandtl-Eyring fluid.

Using the boundary layer assumptions on Eqs. (5.2) – (5.5), the fluid model takes the form:

$$\frac{\partial u}{\partial x} + \frac{\partial v}{\partial y} = 0, \tag{5.8}$$

$$u\frac{\partial u}{\partial x} + v\frac{\partial u}{\partial y} = u_e\frac{\partial u_e}{\partial x} + \frac{A}{\rho c}\frac{\partial^2 u}{\partial y^2} - \frac{A}{2\rho c^3}\left(\frac{\partial u}{\partial y}\right)^2\frac{\partial^2 u}{\partial y^2}$$
$$+ \frac{\sigma B_0^2}{\rho}(u_e - u)\sin^2\theta + \frac{v}{K}(u_e - u), \tag{5.9}$$

$$u\frac{\partial T}{\partial x} + v\frac{\partial T}{\partial y} = \tau D_B\left(\frac{\partial T}{\partial y}\frac{\partial C}{\partial y}\right) + \frac{\tau D_T}{T_\infty}\left(\frac{\partial T}{\partial y}\right)^2 + \alpha\frac{\partial^2 T}{\partial y^2}, \tag{5.10}$$

$$u\frac{\partial C}{\partial x} + v\frac{\partial C}{\partial y} = D_B\frac{\partial^2 C}{\partial y^2} + \frac{D_T}{T_\infty}\frac{\partial^2 T}{\partial y^2}. \tag{5.11}$$

The boundary conditions are defined as

$$u = U_w(x) = ax, \ v = 0, \ T = T_w, C = C_w \ \text{at} \ y = 0,$$
$$u = U_e(x) = bx, \ T \to T_\infty, \ C \to C_\infty \quad \text{at} \ y \to \infty. \tag{5.12}$$

The steam function is specified as:

$$u = \frac{\partial \psi}{\partial y}, \ v = -\frac{\partial \psi}{\partial x}. \tag{5.13}$$

Setting the following similarity transformations

$$\eta = y\sqrt{\frac{a}{\upsilon}}, \quad \psi = \sqrt{a\upsilon}xf(\eta)$$
$$\theta = \frac{T-T_\infty}{T_w-T_\infty}, \quad \varphi = \frac{C-C_\infty}{C_w-C_\infty}. \tag{5.14}$$

Appling the similarity transformation on Eqs (5.8) – (5.12), the following forms are obtained:

$$\alpha f''' - \alpha\beta f''^2 f''' - f'^2 + ff'' - H^2 - M(H -$$
$$f')sin^2\theta - Kp(H - f') = 0, \tag{5.15}$$

$$\theta'' + \Pr[f\theta' + Nb\theta'\varphi' + Nt\theta'^2] = 0, \tag{5.16}$$

$$\varphi'' + LePrf\varphi' \frac{Nt}{Nb}\theta'' = 0. \tag{5.17}$$

The above system is subjected to the following conditions:
$$f = 0, f' = 1, \theta = 1, \varphi = 1 \ at \ \eta = 0 \tag{5.18}$$
$$f' \to 0, \theta \to 0, \varphi \to 0 \ at \ \eta \to \infty.$$

where

$$Le = \frac{\alpha}{D_B}, \beta = \frac{\alpha^3 x^2}{2c^2\upsilon}, \ M = \frac{\sigma B_0^2}{\alpha\rho}, \alpha = \frac{A}{\mu c}, H = \frac{b}{a}, \ Kp = \frac{\upsilon}{Ka}$$

$$Nt = \frac{\tau D_{T(T_W - T_\infty)}}{T_\infty\upsilon}, Nb = \frac{\tau D_{B(C_W - C_\infty)}}{\upsilon}, \ \Pr = \frac{\upsilon}{\alpha 1}, \tag{5.19}$$

in which Le denotes Lewis number, α and β are non-dimensional fluid parameters, M denotes Hartmann number, Pr denotes the Prandtl number, Nt represents thermoporesis parameter, Nb represents Brownian motion parameter, Kp represents porosity parameter, H denotes velocity parameter.

The coefficient of skin friction C_{fx}, the local Nusselt number Nu_x and Sherwood number Sh_x are defined as follows:

$$C_{fx} = \frac{\tau_w}{\frac{1}{2}\rho U^2}, \quad Nu_x = \frac{xq_w}{k(T_w - T_\infty)}, \quad Sh_x = \frac{xq_m}{D_B(C_w - C_\infty)}, \tag{5.20}$$

with

$$\tau_w = \frac{A}{C}\left(\frac{\partial u}{\partial y}\right)_{y=0} - \frac{A}{6C^3}\left(\frac{\partial u}{\partial y}\right)^2_{y=0}, \quad q_w = -k\left(\frac{\partial T}{\partial y}\right)_{y=0}, \quad q_m = D_B\left(\frac{\partial C}{\partial y}\right)_{y=0}. \tag{5.21}$$

Thus using Eq. (5.21) in Eq. (5.20), the following results are acquired

$$\frac{1}{2}Cf_x Re_x^{\frac{1}{2}} = \alpha f''(0) - \frac{\alpha\beta}{3}[f''(0)]^3, \quad Nu_x Re_x^{-\frac{1}{2}} = -\theta'(0),$$

$$Sh_x Re_x^{-\frac{1}{2}} = -\varphi'(0). \tag{5.22}$$

5.3 Numerical Stratagem

Fluid flow issues typically contain complex and nonlinear equations, presenting a challenge to the researcher during solution. These difficulties can be treated numerically, leading to an effective solution. The bvp4c approach, a MATLAB package is used to solve numerically governed ordinary differential equations. To begin the process, first order differential equations are solved.

$$f_1 = f, \tag{5.23}$$

$$f_2 = f_1' = f', \tag{5.24}$$

$$f_3 = f_2' = f'', \tag{5.25}$$

$$f_5 = \theta, \tag{5.26}$$

$$f_6 = f_5' = \theta', \tag{5.27}$$

$$f_8 = \varphi, \tag{5.28}$$

$$f_9 = f_8' = \varphi'. \tag{5.29}$$

Eqs. (5.15) - (5.17) can be presented by:

$$f_4 = f_3' = f''' = \frac{(f_2)^2 - f_1 f_3 - H^2 + M(H - f_2)sin^2\theta + Kp(H - f_2)}{\alpha - \alpha\beta(f_3)^2} \tag{5.30}$$

$$f_7 = f_6' = \theta'' = -Pr(f_1 f_6 + Nb f_6 f_9 + Nt(f_6)^2), \tag{5.31}$$

$$f_{10} = f_9' = \varphi'' = -\frac{Nt}{Nb}f_7 - PrLe f_1 f_9. \tag{5.32}$$

5.4 Graphical Analysis and Discussion

The graphical behaviors of velocity, temperature and concentration due to various factors are depicted and discussed. In this section the outcomes of altering crucial factors such as skin friction coefficient, also as Nusselt & Sherwood numbers are also emphasized. The current study of non-Newtonian fluid flow near a stagnation point is significant in a variety of engineering and industrial applications. Figure 5.2 is sketched to understand the outcome of Hartmann number (M) on velocity profile. This figure demonstrates the lessening impact of Hartmann number (M) with the respect to the velocity sketch. It represent that he bigger the Hartmann number, the greater the resistive force as the thickness of the momentum layer cuts down. Figure 5.3 describes the variation of Prandtl Eyring parameter α for velocity sketch. The increasing influence of Prandtl Eyring parameter α on the velocity sketch is noticeable through the graph. The diversity of Prandtl Eyring parameter (β) in terms of velocity profile is sketched in Figure 5.4. The velocity distribution decreases with the enhancing variation of Prandtl Eyring parameter (β). Figure 5.5 represents the impact of velocity parameter (H) on the respective velocity sketch and the growing effect of the parameter (H) on the velocity sketch is evident through the sketch. Figure 5.6 illustrates the range of porosity parameter (Kp) on the velocity image. This figure signifies the shrinking result of velocity with raised porosity parameter (Kp). The measure of fluid motion like water, oil or gas through a porous medium is directly inclined due to porosity. Increased porosity supplies hold more linked vacant spaces, permitting the fluid movement. Figure 5.7 establishes the effect of angle (θ) in terms of velocity profile. It can been observed that velocity distribution tends to shrunken down with raised θ. The Hartmann number (M) is proportional to $\sin^2\theta$, thus it is also established that the magnetic field shows no influence for velocity curves if $\theta = 0^0$, but affects the flow at $\theta = 90^0$. Figure 5.8 portrays the effect of porosity parameter (Kp) for the noticeable temperature profile. It is analyzed that temperature augments as porosity parameter (Kp) rises. Fig 5.9 depicts the impacts of velocity parameter (H) on temperature profile sketch. It is seen that declining impact of velocity parameter (H) on temperature sketch is obvious. Figure 5.10 shows the impact of θ on temperature sketch and it is detected that as θ rises, temperature sketch goes increasing. Figure 5.11 represents the effects of the Brownian motion parameter (Nb) on temperature profile. This graph exhibit the increasing behavior of temperature sketch with the rising parameter. As increasing kinetic energy of nanoparticles is related with expanded Brownian motion, thus agreeing more particles to move further than the surface and therefore increasing

the temperature. Figure 5.12 demonstrates the effect of thermophoresis factor (*Nt*) for temperature profile. It is monitored that as increase in thermophoresis parameter causes rise in temperature profile. The increase in *Nt* allows for the development of thermophoesis force, which let nanoparticles to travel from hotter to colder section, consequently expanding the temperature profile. Figure 5.13 reveals the consequence of Prandtl number (Pr) recorded for temperature curves. It is seen that temperature shrinkages with growing Prandtl number (Pr) as thermal diffusivity is lesser when compared to momentum diffusivity. Figure 5.14 illustrates outcome of porosity parameter (*Kp*) corresponding to concentration profile. It is perceived that concentration profile growth is associated with the increase of porosity parameter (*Kp*). Figure 5.15 validates the impact of velocity parameter (*H*) on concentration profile. It is assessed that the concentration profile drops as increase in the parameter (*H*) is concerned. Figure 5.16 indicates the impact of angle (θ) relative to concentration sketch. It is investigated that the rise in θ cause escalation in concentration profile Figure 5.17 confirms the variation of Brownian motion factor (*Nb*) for the concentration sketch. The nanoparticle concentration diminished due to the development of the Brownian motion parameter (*Nb*). Figure 5.18 demonstrates the impact of the thermophoretic component (*Nt*) on the concentration sketch. It is analyzed that concentration increase as thermophoretic component (*Nt*) upturns. Figure 5.19 spectacles the variation in Prandtl number (Pr) for concentration curves. The concentration deteriorates when Prandlt number (Pr) tends to rise. Fig 5.20 indicates the behavior of concentration profile when the Lewis number *Le* changes. It is witnessed that with the growth of Lewis number *Le,* the concentration profile decreases. The bigger the Lewis number *Le,* the less impact it has on the nanoparticle volume fraction.

Table 5.1 spectacles the comparison date of skin friction coefficient for various of physical parameters *M*, α, Pr, *Nb*, *Nt* and *Le* when $\beta = H = Kp = \theta = 0$. The acquired values are in promising agreement with the preceding study. Table 5.2 illustrates the impression of various parameters for skin friction, also for Nusselt & Sherwood numbers. The skin friction surges for large values of Prandtl Eyring parameter (α), porosity parameter (*Kp*), Hartmann number (*M*) and angle (θ) and it decays when the values of Prandtl Eyring parameter (β) and velocity flow parameter (*H*) rise. The Nusselt number increases as the values of Prandtl Eyring parameter (α), velocity parameter (*H*) and Prandtl number (Pr) are boosted, however, the opposite is seen for growing values of Prandtl Eyring parameter (β), Hartmann number (*M*), porosity parameter (Kp), Brownian motion parameter (*Nb*), Thermophoresis parameter (*Nt*), Lewis number (*Le*) and θ. The Sherwood number increases as Prandtl Eyring parameter (α), velocity parameter (*H*), Prandtl number (Pr), Brownian motion parameter (*Nb*), Lewis number

(*Le*) are forced to amplify and lessens when associated with aggregated values of Prandtl Eyring parameter (β), Hartmaan number (*M*), Porosity parameter (Kp, thermophoresis parameter (*Nt*) and angle (θ).
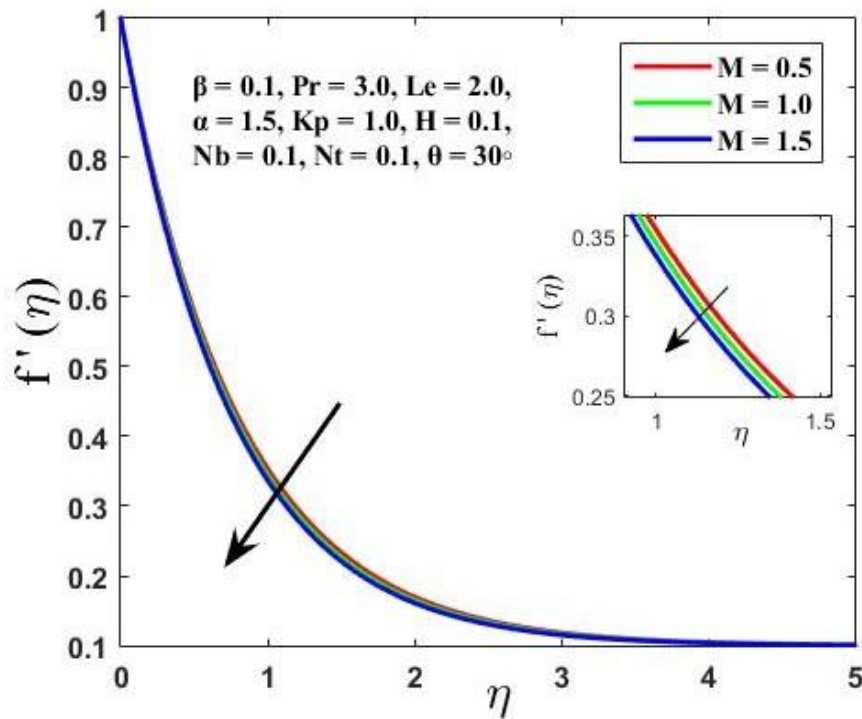
Fig 5.2: Velocity sketch in case of variability in *M*.
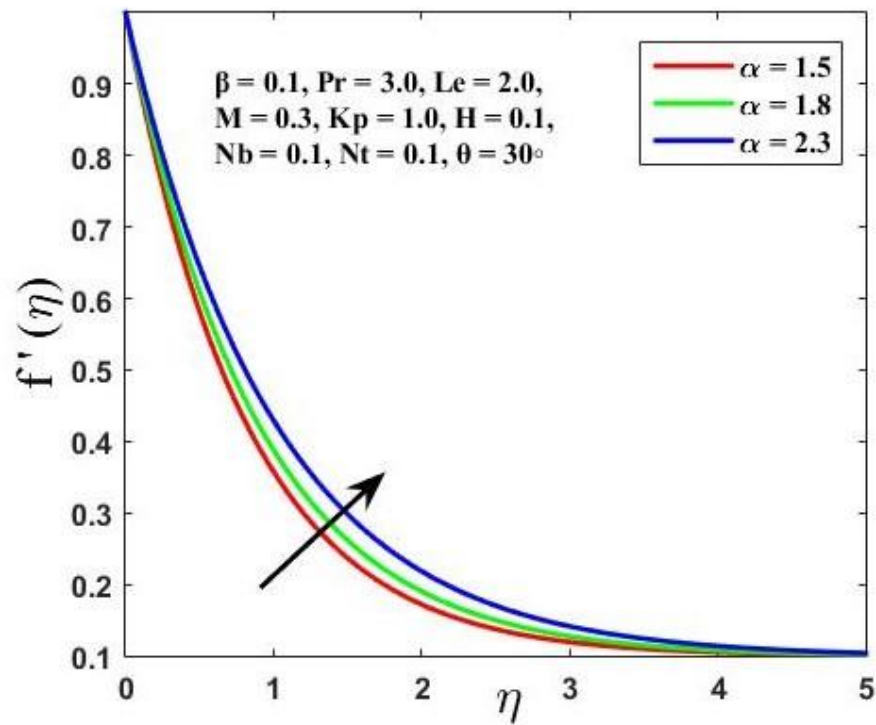
Fig 5.3: Velocity sketch in case of variability in α.
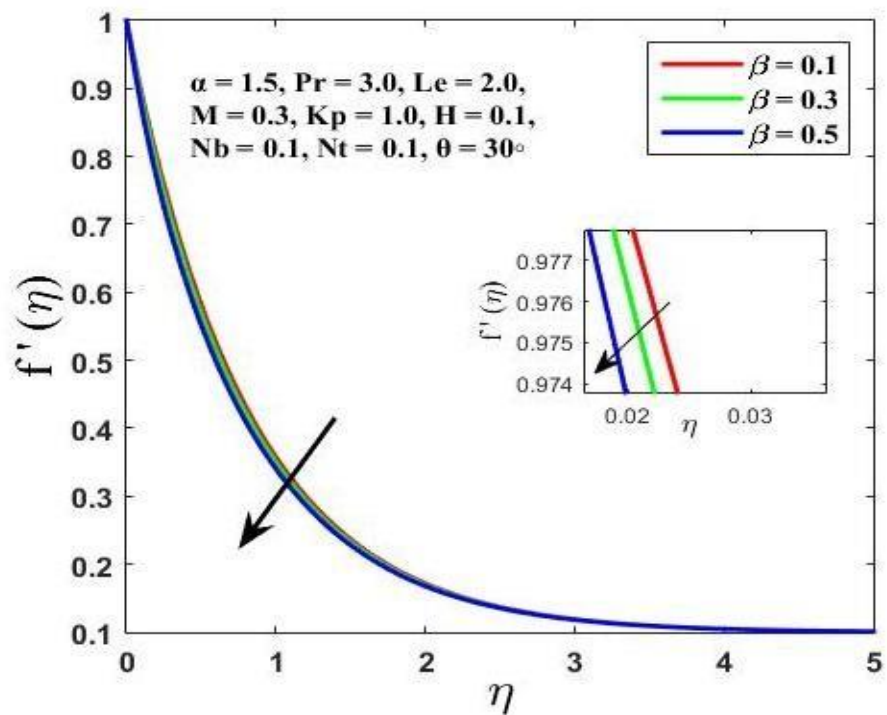
Fig 5.4: Velocity sketch in case of variability in β.
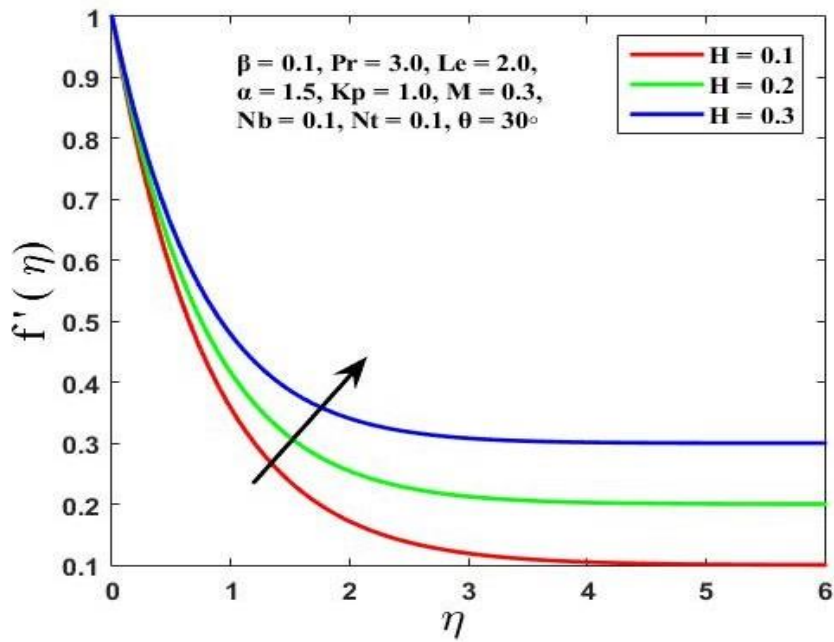
Fig 5.5: Velocity sketch in case of variability in *H*.
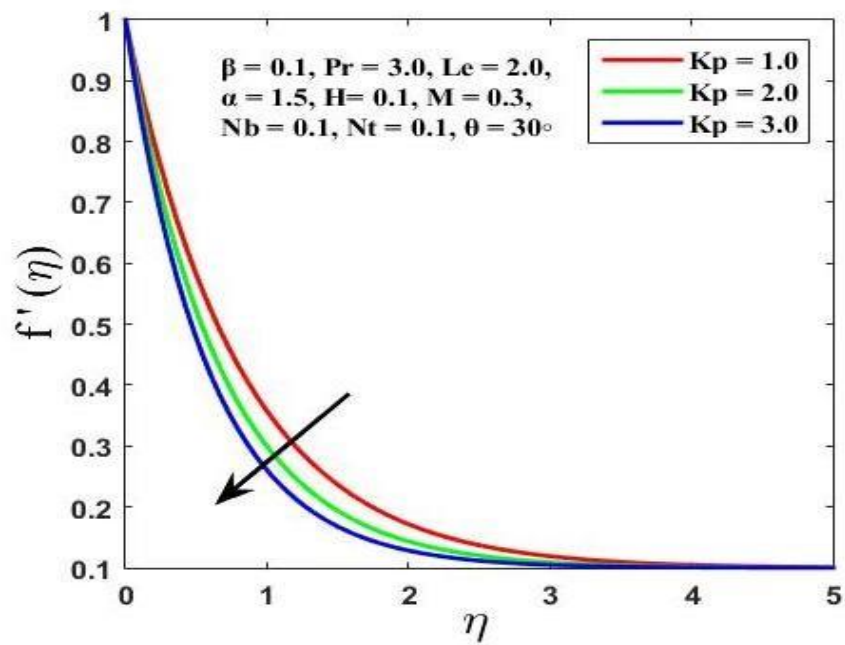
Fig 5.6: Velocity sketch in case of variability in *Kp*.
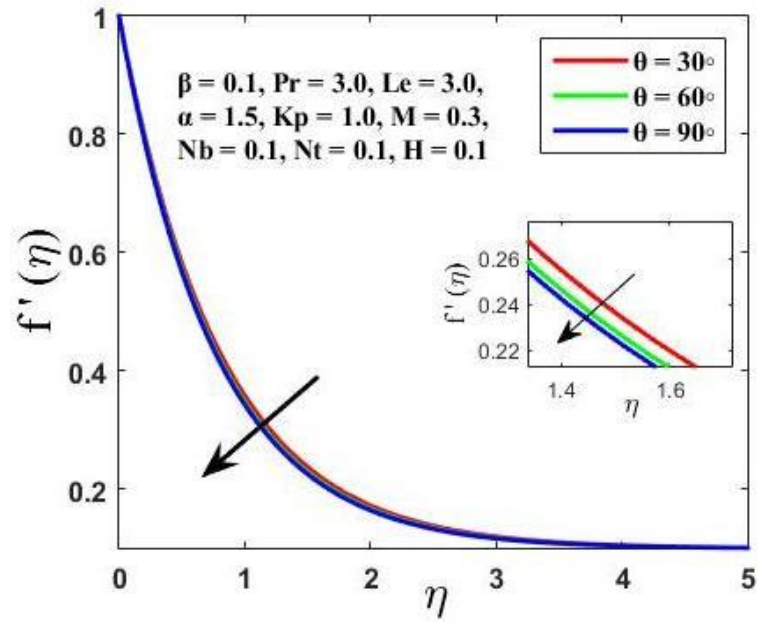
Fig 5.7: Velocity sketch in case of variability in θ.
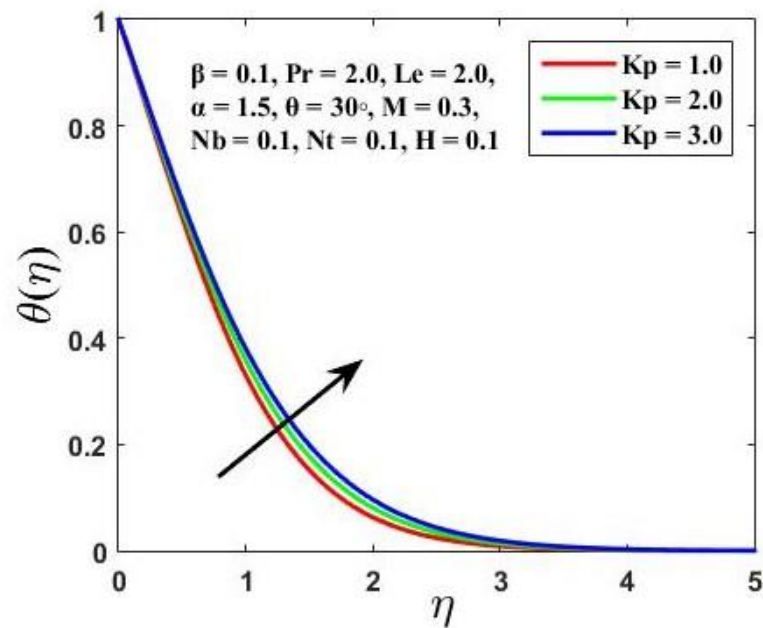
Fig 5.8: Temperature sketch in case of variability in Kp.
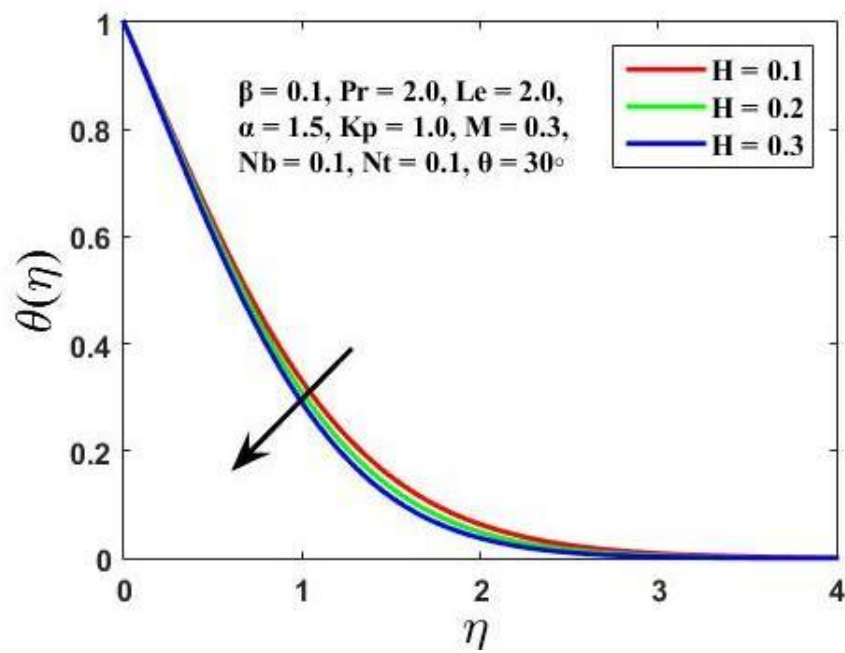
Fig 5.9: Temperature sketch in case of variability in *H*.
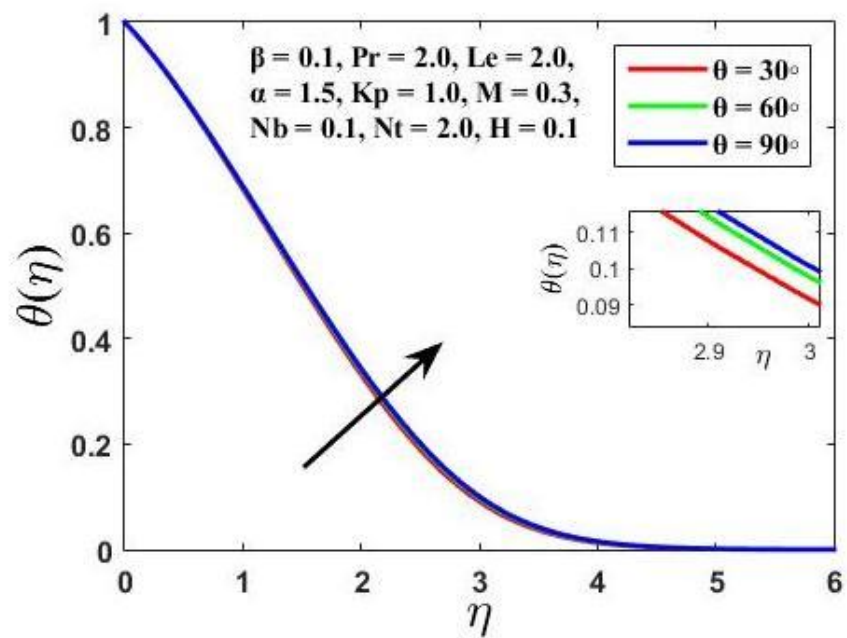
Fig 5.10: Temperature sketch in case of variability in *θ*.
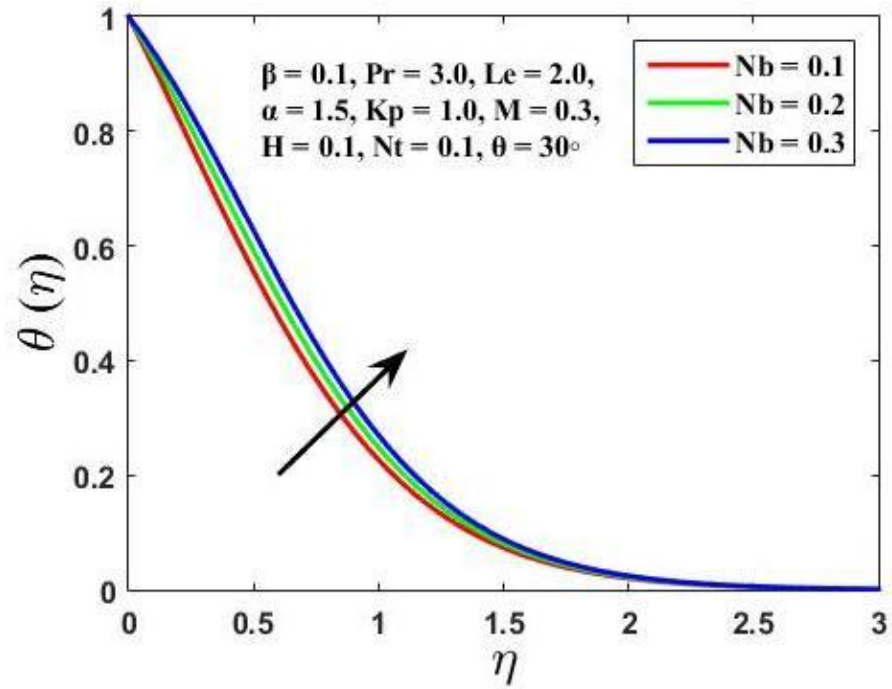
Fig 5.11: Temperature sketch in case of variability in *Nb*.
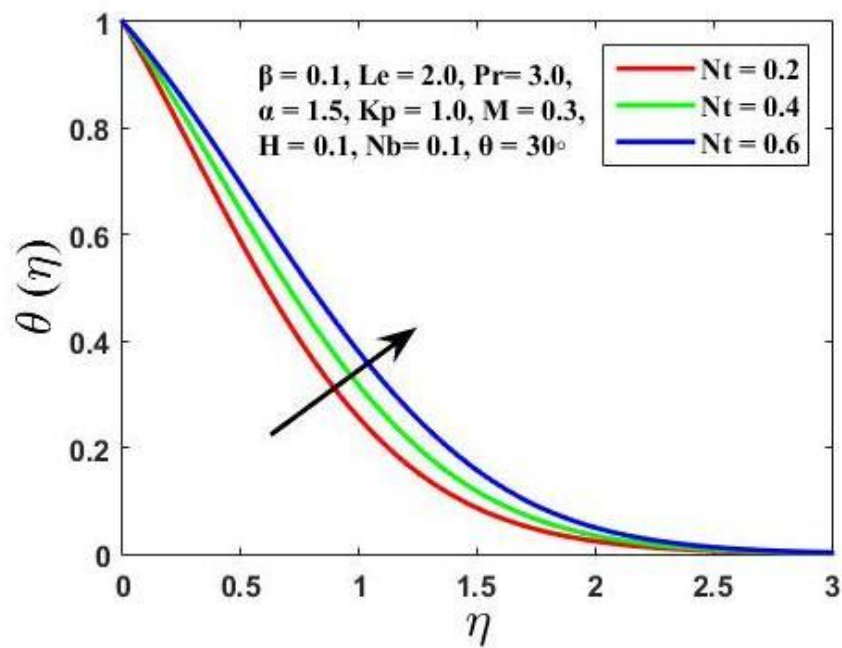
Fig 5.12: Temperature sketch in case of variability in *Nt*.
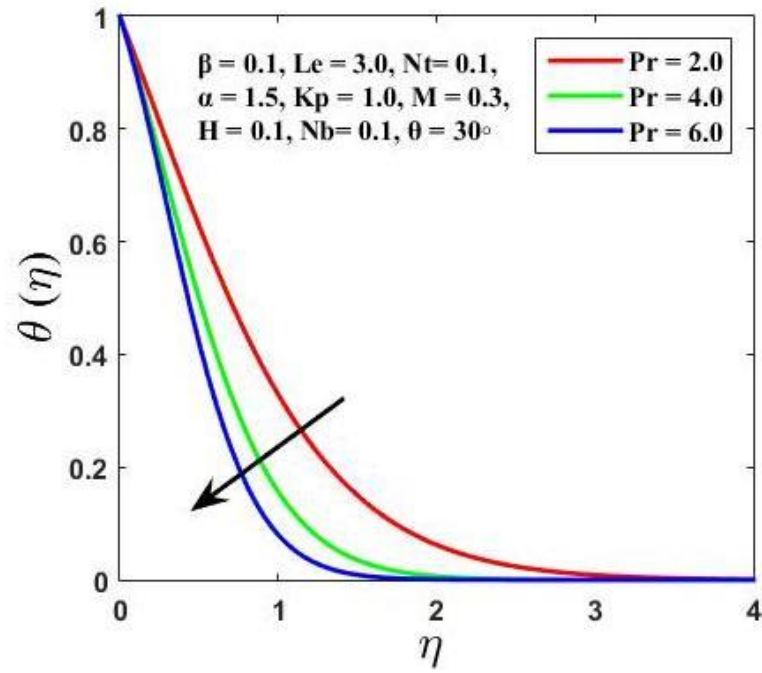
Fig 5.13: Temperature sketch in case of variability in Pr.
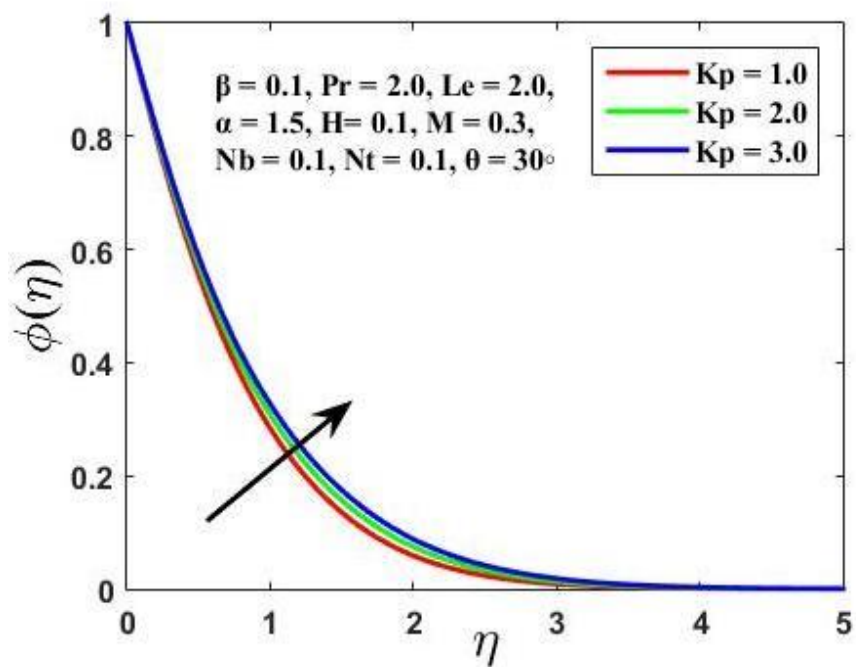
Fig 5.14: Concentration sketch in case of variability in *Kp*.
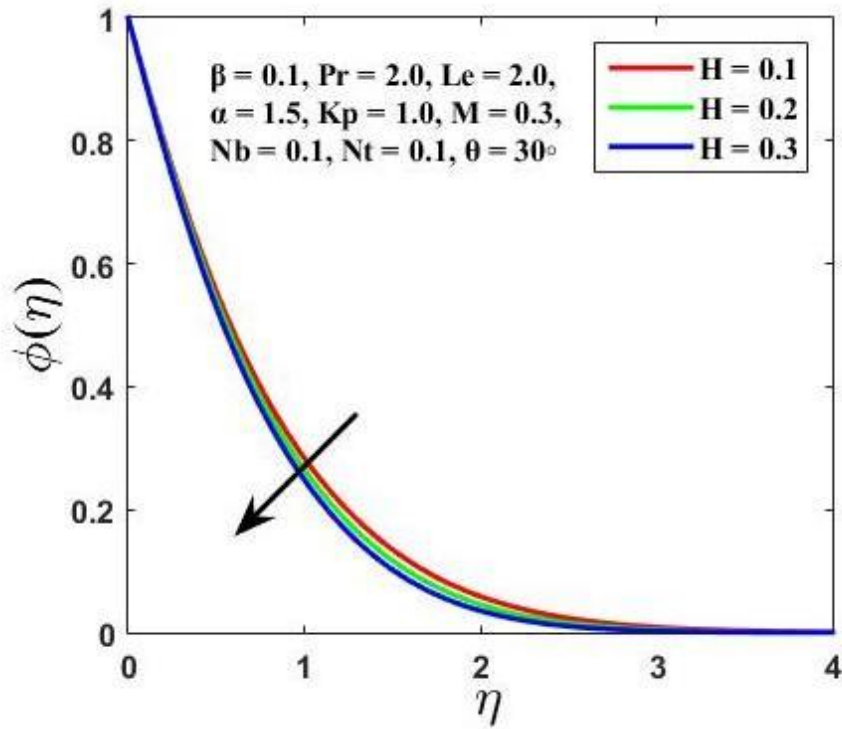
Fig 5.15: Concentration sketch in case of variability in *H*.
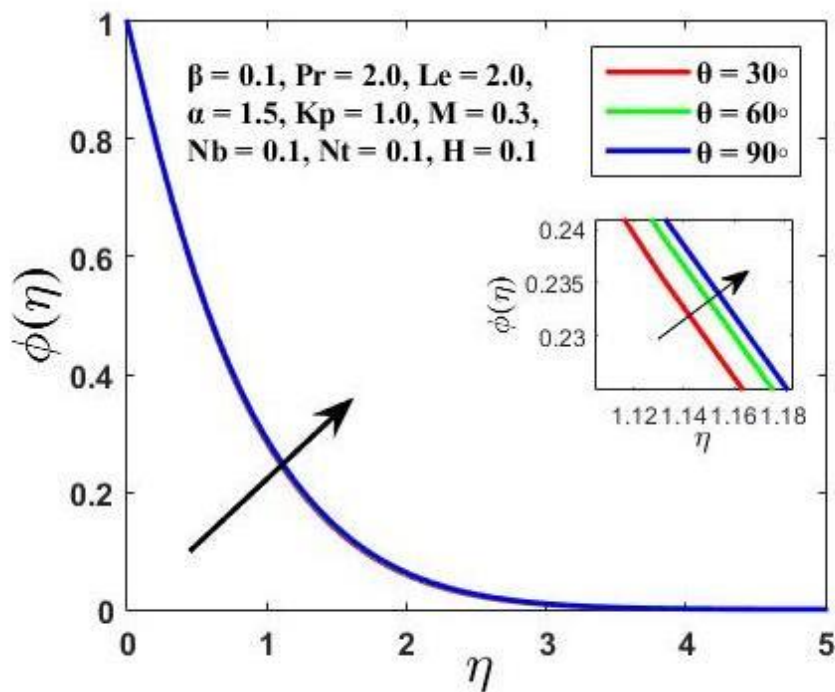
Fig 5.16: Concentration sketch in case of variability in *θ*.
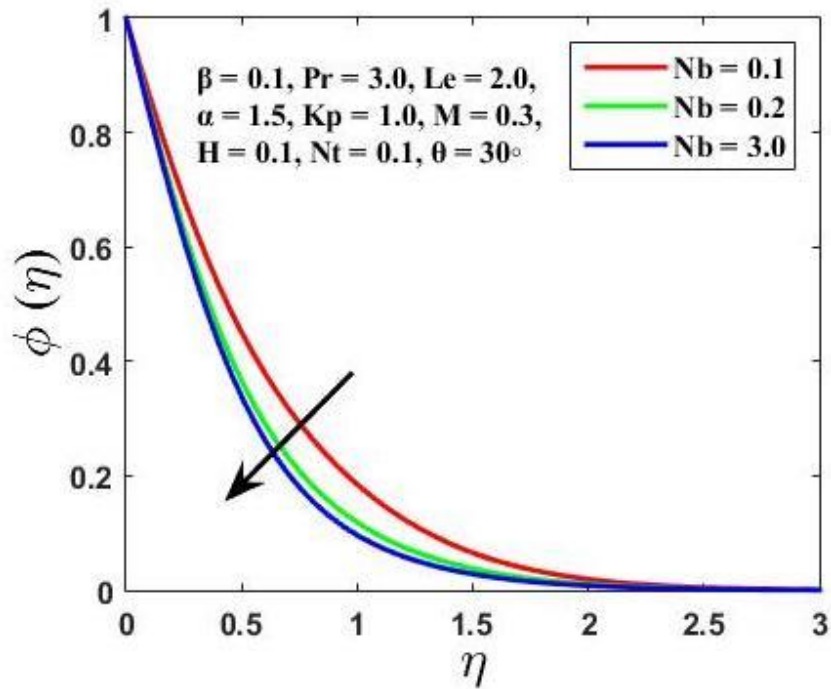
Fig 5.17: Concentration sketch in case of variability in *Nb*.
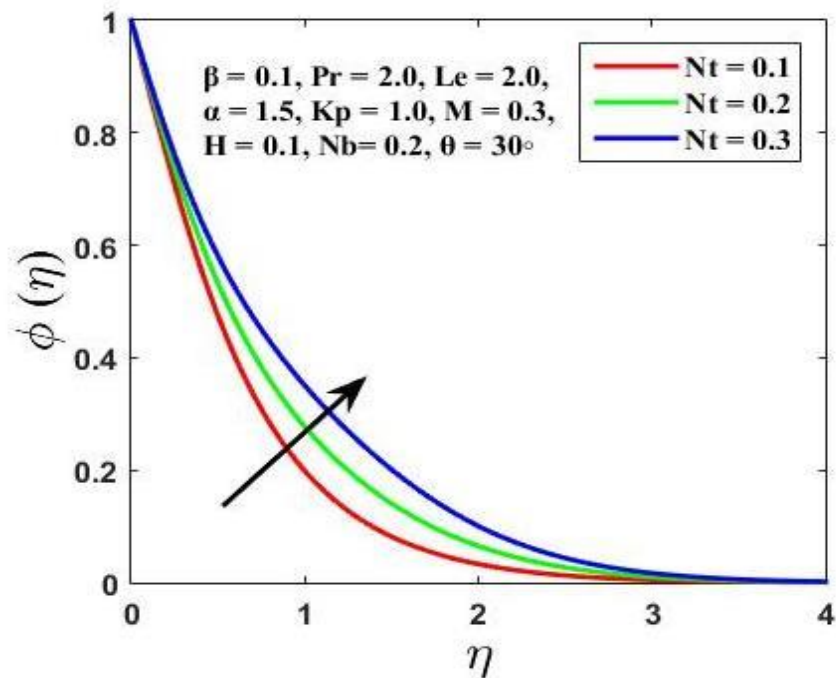
Fig 5.18: Concentration sketch in case of variability in *Nt*.
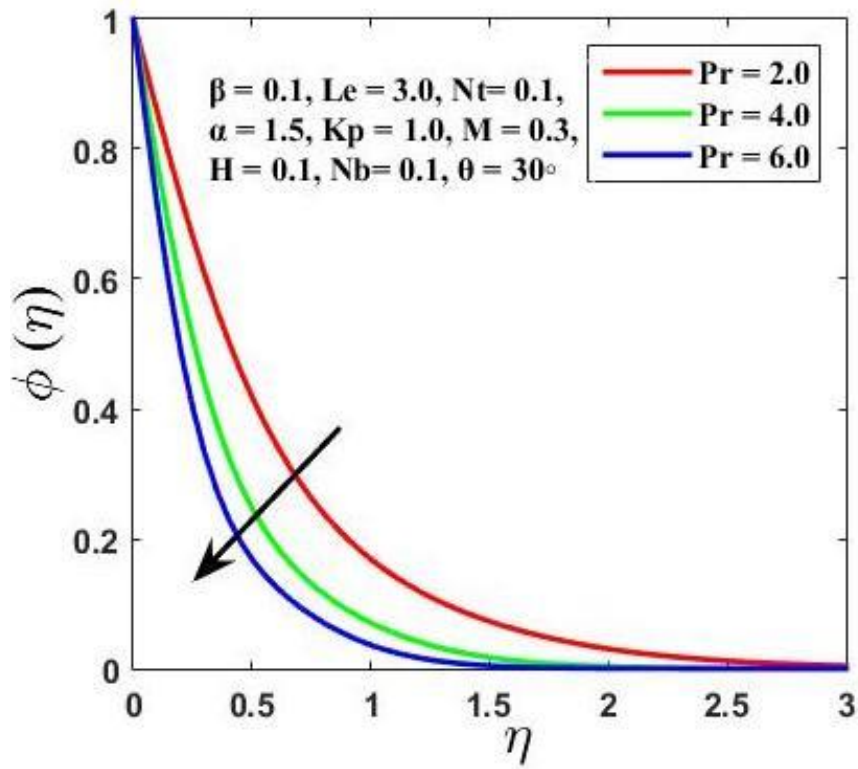
Fig 5.19: Concentration sketch in case of variability in Pr.
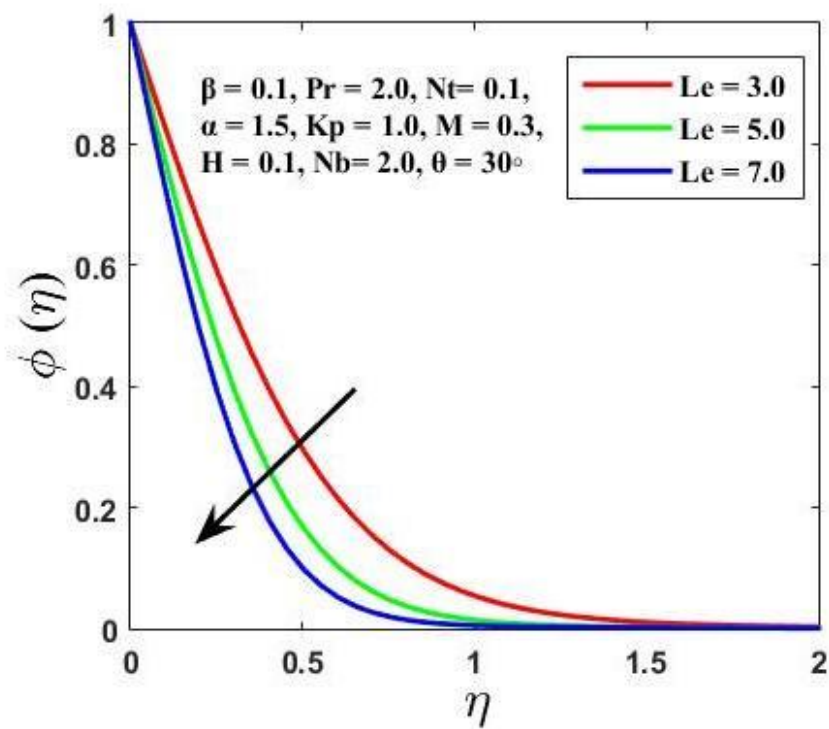
Fig 5.20: Concentration sketch in case of variability in *Le*.

Table 5.1: Comparative values of skin friction coefficient for M if $\alpha = 1$, $\beta = H = Kp = \theta = 0$.

M	Fatehzadeh *et al.* [127]	Akbar *et al.* [128]	Abdelmalek *et al.* [126]	Present Results
0	-1	-1	-1.004	-1.0014
0.5	-	-1.11803	-1.1180	-1.1181
1.0	-1.41412	-1.41421	-1.4140	-1.4142
5.0	-2.44948	-2.44949	-2.4494	-2.4495
10	-3.31662	-3.31663	-3.3168	-3.3166
50	-7.14142	-	-4.4143	-7.1414
100	-10.0499	-10.04889	-10.0502	-10.0499
500	-22.383	-22.38303	-22.3831	-22.3830
1000	-31.6368	-31.63859	-31.6387	-31.6386

Table 5.2: Computed values of $\left| -\alpha f''(0) - \frac{\alpha\beta}{3}\left(f''(0)\right)^3 \right|, -\theta'(0), -\varphi'(0)$ for numerous values of physical parameter.

α	B	M	Kp	H	Nb	Nt	Pr	Le	θ	Skin friction coefficient	Nusselt number	Sherwood number
1.5	0.1	0.3	1.0	0.1	0.1	0.1	2.0	3.0	30	1.6273	0.7221	1.4426
2.0										1.8849	0.7453	1.4770
3.0										2.3167	0.7737	1.5186
1.5	0.1									1.6273	0.7221	1.4426
	0.2									1.6065	0.7191	1.4376
	0.3									1.5824	0.7155	1.4314
	0.4									1.5516	0.7106	1.4229
	0.1	0.3								1.6273	0.7221	1.4426
		0.5								1.6450	0.7202	1.4399
		0.6								1.6538	0.7193	1.4385
		0.8								1.6711	0.7175	1.4358
		0.3	1.0							1.6273	0.7221	1.4426
			2.0							1.9479	0.6892	1.3928
			3.0							2.2169	0.6628	1.3517
			4.0							2.4506	0.6407	1.3164
			1.0	0.1						1.6273	0.7221	1.4426
				0.2						1.4984	0.7459	1.4750
				0.4						1.1983	0.7902	1.5372

				0.6						0.8457	0.8312	1.5966
				0.1	0.1					1.6273	0.7221	1.4426
					0.2					1.6273	0.6253	1.6176
					0.3					1.6273	0.5397	1.6727
					0.5					1.6273	0.3984	1.7116
					0.1	0.1				1.6273	0.7221	1.4426
						0.2				1.6273	0.6670	1.2385
						0.3				1.6273	0.6171	1.0932
						0.5				1.6273	0.5311	0.9367
						0.1	2.0			1.6273	0.7221	1.4426
							3.0			1.6273	0.8253	1.8935
							4.0			1.6273	0.8739	2.3020
							5.0			1.6273	0.8883	2.6810
							2.0	3.0		1.6273	0.7221	1.4426
								4.0		1.6273	0.7139	1.7817
								5.0		1.6273	0.7084	2.0750
								7.0		1.6273	0.7012	2.5751
								3.0	30	1.6273	0.7221	1.4426
									45	1.6538	0.7193	1.4385
									60	1.6798	0.7166	1.4344
									90	1.7053	0.7140	1.4304

CHAPTER 6

CONCLUSION AND FUTURE WORK

6.1   Concluding remarks

The current study is based on stagnation point flow of viscoelastic nanofluid. The nanoparticles can influence the viscoelastic properties of the fluid, resulting in a new kind of fluid with unique combination of features. The study of viscoelastic fluid for stagnation point flow has gained importance, due to the prediction of skin friction and mass/heat transfer near stagnation regions. These fluids have a wide range of applications, including the lubrication, environmental remediation, petroleum industry, surface coating, biomedical, electronics and cooling systems.

The stagnation point flow of nanofluid is investigated in the presence of porosity effect and inclined magnetic field and the fluid is flowing across a stretched surface. The system of equations is expressed as a set of partial differential equations, which are then transformed into simpler ordinary differential equations. The problem's numerical investigation reveals the major results that can help in future studies. The velocity profiles decrease with each upgrade of the parameters, Hartmann number (M), porosity parameter (Kp), Prandtl Eyring parameter (β) and the angle (θ). The same uprising behavior is observed in terms of velocity for the Prandtl Eyring parameter (α) and velocity parameter (H). The temperature profile rises with the enlargement of the porosity parameter (Kp), angle (θ), Brownian motion parameter (Nb) and Thermophoresis parameter (Nt) but few other parameters show opposite trend for temperature. As velocity parameter (H) and Prandtl number (Pr) grow, the temperature profile decreases. The results are also obtained for concentration profile by changing the parameters. As the

porosity parameter (*Kp*), angle (*θ*) and Thermophoresis parameter (*Nt*) are enhanced, the concentration distribution grows while decrease in concentration profile with the rise of the parameters such as velocity parameter (*H*), Brownian motion parameter (*Nb*), Lewis number (*Le*), and Prandtl number (Pr) is substantial. When Prandtl Eyring parameter (*α*), Hartmann number (*M*), porosity parameter (*Kp*) and angle (*θ*) are increased, the skin friction exhibits an upward trend while when Prandtl Eyring parameter (*β*) and velocity parameter (*H*) are raised, the skin friction coefficient displays a reversal behavior. The Nusselt number rises by increasing the values of Prandtl Eyring parameter (*α*), velocity parameter (*H*), and Prandtl number (Pr) and declines with increasing values of Hartmann number (*M*), Prandtl Eyring parameter (*β*), porosity parameter (*Kp*), thermophoresis parameter (*Nt*), Brownian motion parameter (*Nb*), Lewis number (*Le*) and the angle (*θ*). The Sherwood number increases with increasing values of Prandtl Eyring parameter (*α*), velocity parameter (*H*), Brownian motion parameter (*Nb*), Prandtl number (Pr), Lewis number (*Le*) and decreases with enhanced values of Prandtl Eyring parameter (*β*), Hartmann number (*M*), porosity parameter (*Kp*), thermophoresis parameter (*Nt*) and angle (*θ*).

6.2   Proposed Future Work

The stagnation point flow of nano-fluid over a stretching surface in the presence of inclined MHD was investigated in this study. However, there is still space to improve the present work in order to address other problems. The following are some interesting future investigations that might be conducted.

- Non-Newtonian fluids are a part of numerous applications in industry and engineering. The current study can be extended to other kinds of non-Newtonian fluids in different geometries.
- The stagnation point flow of Prandtl-Eyring fluid can be investigated while flowing over a curved surface with the presence of velocity slip.
- The nanofluid flow of Prandtl-Eyring fluid can explored while flowing between two oscillating parallel plates.

References:

1. Choi, S. U. S. (1995). Enhancing thermal conductivity of fluids with nanoparticles. *Developments and Applications of Non-Newtonian Flows*, 231, 99– 105.

2. Lee, S., Choi, S. S., Li, S. A., & Eastman, J. A. (1999). Measuring thermal conductivity of fluids containing oxide nanoparticles. *The Journal of Heat Transfer*, 121 2, 280-289.

3. Xie, H., Fujii, M., & Zhang, X. (2005). Effect of interfacial nanolayer on the effective thermal conductivity of nanoparticle-fluid mixture. *International Journal of Heat and Mass Transfer*, 48(14), 2926-2932.

4. Santra, A. K., Sen, S., & Chakraborty, N. (2008). Study of heat transfer augmentation in a differentially heated square cavity using copper–water nanofluid. *International Journal of Thermal Sciences*, 47(9), 1113-1122.

5. Ghadimi, A., Saidur, R., & Metselaar, H. S. C. (2011). A review of nanofluid stability properties and characterization in stationary conditions. *International journal of heat and mass transfer*, 54(17), 4051-4068.

6. Hendraningrat, L., Li, S., & Torsæter, O. (2013). A coreflood investigation of nanofluid enhanced oil recovery. *Journal of Petroleum Science and Engineering*, 111, 128-138.

7. Mahian, O., Kianifar, A., Kleinstreuer, C., Moh'd A, A. N., Pop, I., Sahin, A. Z., & Wongwises, S. (2013). A review of entropy generation in nanofluid flow. *International Journal of Heat and Mass Transfer*, 65, 514-532.

8. Sheikholeslami, M., & Ganji, D. D. (2015). Nanofluid flow and heat transfer between parallel plates considering Brownian motion using DTM. *Computer Methods in Applied Mechanics and Engineering*, 283, 651-663.

9. Rehman, S. U., Haq, R. U., Khan, Z. H., & Lee, C. (2016). Entropy generation analysis for non-Newtonian nanofluid with zero normal flux of nanoparticles at the stretching surface. *Journal of the Taiwan Institute of Chemical Engineers*, 63, 226-235.

10. Gireesha, B. J., Kumar, K. G., Ramesh, G. K., & Prasannakumara, B. C. (2018). Nonlinear convective heat and mass transfer of Oldroyd-B nanofluid over a stretching sheet in the presence of uniform heat source/sink. *Results in Physics*, 9, 1555-1563.

11. Tong, Y., Lee, H., Kang, W., & Cho, H. (2019). Energy and exergy comparison of a flat- plate solar collector using water, Al2O3 nanofluid, and CuO nanofluid. *Applied Thermal Engineering*, 159, 113959.

12. Agi, A., Junin, R., Abdullah, M. O., Jaafar, M. Z., Arsad, A., Sulaiman, W. R. W., & Azli, N. B. (2020). Application of polymeric nanofluid in enhancing oil recovery at reservoir condition. *Journal of Petroleum Science and Engineering*, 194, 107476.

13. Ahmadi, M. H., Mohseni-Gharyehsafa, B., Ghazvini, M., Goodarzi, M., Jilte, R. D., & Kumar, R. (2020). Comparing various machine learning approaches in modeling the dynamic viscosity of CuO/water nanofluid. *Journal of Thermal Analysis and Calorimetry*, 139, 2585-2599.

14. Saffarian, M. R., Moravej, M., & Doranehgard, M. H. (2020). Heat transfer enhancement in a flat plate solar collector with different flow path shapes using nanofluid. *Renewable Energy*, 146, 2316-2329.

15. Sheikholeslami, M., & Farshad, S. A. (2021). Numerical simulation of effect of non-uniform solar irradiation on nanofluid turbulent flow. *International Communications in Heat and Mass Transfer*, 129, 105648.

16. Ma, T., Guo, Z., Lin, M., & Wang, Q. (2021). Recent trends on nanofluid heat transfer machine learning research applied to renewable energy. *Renewable and Sustainable Energy Reviews*, 138, 110494.

17. Stewartson, K. (1981). D'Alembert's Paradox. *SIAM Review*, *23*(3), 308–343.

18. Anderson, J. D. (2005). Ludwig Prandtl's boundary layer. *Physics today*, 58(12), 42-48.

19. Taylor, G. I. (1934). The formation of emulsions in definable fields of flow. *Proceedings of the Royal Society of London. Series A, containing papers of a mathematical and physical character*, 146(858), 501-523.

20. Hiemenz, K. (1911). "Die Grenzschicht an einem in den gleichformigen ¨ Flussigkeitsstrom eingetauchten geraden Kreiszylinder. Dingl. Poly- ¨ tech," J, 326, 321–410.

21. Ariel, P. D. (1995). Stagnation point flow of a viscoelastic fluid towards a moving plate. *International journal of engineering science*, 33(11), 1679-1687.

22. Mahapatra, T. R., & Gupta, A. S. (2004). Stagnation-point flow of a viscoelastic fluid towards a stretching surface. *International Journal of Non-Linear Mechanics*, 39(5), 811-820.

23. Layek, G. C., Mukhopadhyay, S., & Samad, S. A. (2007). Heat and mass transfer analysis for boundary layer stagnation-point flow towards a heated porous stretching sheet with heat absorption/generation and suction/blowing. *International communications in heat and mass transfer*, 34(3), 347-356.

24. Labropulu, F., Li, D., & Pop, I. (2010). Non-orthogonal stagnation-point flow towards a stretching surface in a non-Newtonian fluid with heat transfer. *International Journal of Thermal Sciences*, 49(6), 1042-1050.

25. Roşca, N. C., & Pop, I. (2013). Mixed convection stagnation point flow past a vertical flat plate with a second order slip: heat flux case. *International Journal of Heat and Mass Transfer*, 65, 102-109.

26. Malvandi, A., Hedayati, F., & Ganji, D. D. (2014). Slip effects on unsteady stagnation point flow of a nanofluid over a stretching sheet. *Powder Technology*, 253, 377-384.

27. Haq, R. U., Nadeem, S., Khan, Z. H., & Akbar, N. S. (2015). Thermal radiation and slip effects on MHD stagnation point flow of nanofluid over a stretching sheet. *Physica E: Low-dimensional systems and nanostructures*, 65, 17-23.

28. Hayat, T., Hussain, Z., Alsaedi, A., & Asghar, S. (2016). Carbon nanotubes effects in the stagnation point flow towards a nonlinear stretching sheet with variable thickness. *Advanced Powder Technology*, 27(4), 1677-1688.

29. Bano, A., Sajid, M., Mahmood, K., & Rana, M. A. (2019). An oblique stagnation point flow towards a stretching cylinder with heat transfer. *Physica Scripta*, 95(1), 015704.

30. Ashraf, K., Siddique, I., & Hussain, A. (2020). Impact of thermophoresis and Brownian motion on non-Newtonian nanofluid flow with viscous dissipation near stagnation point. *Physica Scripta*, 95(5), 055217.

31. Han, Q., Sun, C., Tao, Y., Li, Z., Zhang, Y., & Chen, Y. (2020). Thermal protection of a hypersonic vehicle by modulating stagnation-point heat flux. *Aerospace Science and Technology*, 98, 105673.

32. Khan, M., El Shafey, A. M., Salahuddin, T., & Khan, F. (2020). Chemically Homann stagnation point flow of Carreau fluid. *Physica A: Statistical Mechanics and its Applications*, 551, 124066.

33. Awan, A. U., Aziz, M., Ullah, N., Nadeem, S., & Abro, K. A. (2021). Thermal analysis of oblique stagnation point flow with slippage on second-order fluid. *Journal of Thermal Analysis and Calorimetry*, 1-13.

34. Riaz, N., Qasim, M., Afridi, M. I., & Hussanan, A. (2021). Analysis of three-dimensional stagnation point flow over a radiative surface. *International Communications in Heat and Mass Transfer*, 127, 105538.

35. Alhamaly, A. S., Khan, M., Shuja, S. Z., Yilbas, B. S., & Al-Qahtani, H. (2021). Axisymmetric stagnation point flow on linearly stretching surfaces and heat transfer:

Nanofluid with variable physical properties. *Case Studies in Thermal Engineering*, 24, 100839.

36. Alfvén, H. (1942). Existence of electromagnetic-hydrodynamic waves. *Nature*, 150(3805), 405-406.

37. Abdou, M. (2007). Introduction to MHD and applications to Thermofluids of fusion blankets": Lecture notes. *Institute for Plasma Research (IPR), Gandhinagar, India.*

38. Raptis, A., Perdikis, C., & Takhar, H. S. (2004). Effect of thermal radiation on MHD flow. *Applied Mathematics and computation*, 153(3), 645-649.

39. Turkyilmazoglu, M. (2012). MHD fluid flow and heat transfer due to a stretching rotating disk. *International journal of thermal sciences*, 51, 195-201.

40. Hayat, T., Imtiaz, M., Alsaedi, A., & Kutbi, M. A. (2015). MHD three-dimensional flow of nanofluid with velocity slip and nonlinear thermal radiation. *Journal of Magnetism and Magnetic Materials*, 396, 31-37.

41. Waqas, M., Farooq, M., Khan, M. I., Alsaedi, A., Hayat, T., & Yasmeen, T. (2016). Magnetohydrodynamic (MHD) mixed convection flow of micropolar liquid due to nonlinear stretched sheet with convective condition. *International Journal of Heat and Mass Transfer*, 102, 766-772.

42. Ghasemi, K., & Siavashi, M. (2017). MHD nanofluid free convection and entropy generation in porous enclosures with different conductivity ratios. *Journal of Magnetism and Magnetic Materials*, 442, 474-490.

43. Gaffar, S. A., Prasad, V. R., Bég, O. A., Khan, M. H. H., & Venkatadri, K. (2018). Radiative and magnetohydrodynamics flow of third-grade viscoelastic fluid past an isothermal inverted cone in the presence of heat generation/absorption. *Journal of the Brazilian Society of Mechanical Sciences and Engineering*, 40, 1-19.

44. Shah, Z., Islam, S., Gul, T., Bonyah, E., & Khan, M. A. (2018). The electrical MHD and hall current impact on micropolar nanofluid flow between rotating parallel plates. *Results in physics*, 9, 1201-1214.

45. Ahmed, S. E., Mansour, M. A., Hussein, A. K., Mallikarjuna, B., Almeshaal, M. A., & Kolsi, L. (2019). MHD mixed convection in an inclined cavity containing adiabatic obstacle and filled with Cu–water nanofluid in the presence of the heat generation and partial slip. *Journal of Thermal Analysis and Calorimetry*, 138, 1443-1460.

46. Yasmin, A., Ali, K., & Ashraf, M. (2020). Study of heat and mass transfer in MHD flow of micropolar fluid over a curved stretching sheet. *Scientific reports*, 10(1), 4581.

47. Khan, M., Salahuddin, T., Malik, M. Y., Alqarni, M. S., & Alqahtani, A. M. (2020). Numerical modeling and analysis of bioconvection on MHD flow due to an upper paraboloid surface of revolution. *Physica A: Statistical Mechanics and its Applications*, 553, 124231.

48. Gopal, D., Saleem, S., Jagadha, S., Ahmad, F., Almatroud, A. O., & Kishan, N. (2021). Numerical analysis of higher order chemical reaction on electrically MHD nanofluid under influence of viscous dissipation. *Alexandria Engineering Journal*, 60(1), 1861-1871.

49. Shashikumar, N. S., Madhu, M., Sindhu, S., Gireesha, B. J., & Kishan, N. (2021). Thermal analysis of MHD Williamson fluid flow through a microchannel. *International Communications in Heat and Mass Transfer*, 127, 105582.

50. Khan, M., Salahuddin, T., & Elmasry, Y. (2021). A brief study on MHD viscoelastic nanofluid flow due to variable thick surface with zero normal flux. *Case Studies in Thermal Engineering*, 26, 101175.

51. Theodorakakos, A., Ous, T., Gavaises, M., Nouri, J. M., Nikolopoulos, N., & Yanagihara, H. (2006). Dynamics of water droplets detached from porous surfaces of relevance to PEM fuel cells. *Journal of colloid and interface science*, 300(2), 673-687.

52. Huan, Z., Fratila-Apachitei, L. E., Apachitei, I., & Duszczyk, J. (2012). Porous NiTi surfaces for biomedical applications. *Applied Surface Science*, 258(13), 5244-5249.

53. Haghighi, E., & Or, D. (2015). Thermal signatures of turbulent airflows interacting with evaporating thin porous surfaces. *International Journal of Heat and Mass Transfer*, 87, 429-446.

54. Gu, H., Wang, C., Gong, S., Mei, Y., Li, H., & Ma, W. (2016). Investigation on contact angle measurement methods and wettability transition of porous surfaces. *Surface and Coatings Technology*, 292, 72-77.

55. Choi, M., Son, G., & Shim, W. (2017). Numerical simulation of droplet impact and evaporation on a porous surface. *International Communications in Heat and Mass Transfer*, 80, 18-29.

56. Eid, M. R., Mahny, K. L., Muhammad, T., & Sheikholeslami, M. (2018). Numerical treatment for Carreau nanofluid flow over a porous nonlinear stretching surface. *Results in physics*, 8, 1185-1193.

57. Umavathi, J. C., & Hemavathi, K. (2019). Flow and heat transfer of composite porous medium saturated with nanofluid. *Propulsion and Power Research*, 8(2), 173-181.

58. Hayat, T., Haider, F., Alsaedi, A., & Ahmad, B. (2020). Unsteady flow of nanofluid through porous medium with variable characteristics. *International Communications in heat and mass transfer*, 119, 104904.

59. Wang, Y., Zeng, W., Mei, D., & Zhang, X. (2020). Numerical modeling of microchannel reactors with gradient porous surfaces for hydrogen production based on fractal geometry. *International Journal of Hydrogen Energy*, 45(38), 19733-19744.

60. Al-Farhany, K., & Abdulsahib, A. D. (2021). Study of mixed convection in two layers of saturated porous medium and nanofluid with rotating circular cylinder. *Progress in Nuclear Energy*, 135, 103723.

61. Sajjad, U., Hussain, I., Hamid, K., Bhat, S. A., Ali, H. M., & Wang, C. C. (2021). A deep learning method for estimating the boiling heat transfer coefficient of porous surfaces. *Journal of Thermal Analysis and Calorimetry*, 145, 1911-1923.

62. Zhang, G., Liu, B., Xu, L., Zhang, R., He, Y., & Wang, F. (2021). How porous surfaces influence the nucleation and growth of methane hydrates. *Fuel*, 291, 120142.

63. Sajid, T., Jamshed, W., Safdar, R., Hussain, S. M., Shahzad, F., Bilal, M., & Pasha, A. A. (2022). Features and aspects of radioactive flow and slippage velocity on rotating two-phase Prandtl nanofluid with zero mass fluxing and convective constraints. *International Communications in Heat and Mass Transfer*, 136, 106180.

64. Kamran, A., & Azhar, E. (2022). Numerical outlook of a viscoelastic nanofluid in an inclined channel via Keller box method. *International Communications in Heat and Mass Transfer, 137,106260.*

65. Hamad, N. H., Wakif, A., & Alshehri, A. (2022). Towards the dynamics of a radiative-reactive magnetized viscoelastic nanofluid involving gyrotactic microorganisms and flowing over a vertical stretching sheet under multiple convective and stratification constraints. *Waves in Random and Complex Media*, https://doi.org/10.1080/17455030.2022.2100944.

66. Alqarni, M. S., Waqas, H., Alghamdi, M., & Muhammad, T. (2022). Importance of bioconvection in 3D viscoelastic nanofluid flow due to exponentially stretching surface with nonlinear radiative heat transfer and variable thermal conductivity. *Journal of Thermal Analysis and Calorimetry*, 147(7), 4805-4819.

67. Bouslimi, J., Alkathiri, A. A., Althagafi, T. M., Jamshed, W., & Eid, M. R. (2022). Thermal properties, flow and comparison between Cu and Ag nanoparticles suspended in sodium alginate as Sutterby nanofluids in solar collector. *Case Studies in Thermal Engineering*, 39, 102358.

68. Waqas, H., Khan, S. A., Bukhari, F. F., Muhammad, T., & Alshehri, A. (2023). Heat transfer on non-Newtonian nanofluid flow with bioconvection aspects over rotating thin needle by variable viscosity. *Waves in Random and Complex Media*, https://doi.org/10.1080/17455030.2023.2203770.

69. Bayareh, M. (2023). An overview of non-Newtonian nanofluid flow in macro-and micro-channels using two-phase schemes. *Engineering Analysis with Boundary Elements*, 148, 165-175.

70. Mustafa, Z., Javed, T., Hayat, T., & Alsaedi, A. (2023). Unsteady nanofluid flow over a cone featuring mixed convection and variable viscosity. *Heliyon*., https://doi.org/10.1016/j.heliyon.2023.e16393.

71. Aljaloud, A. S. M., Manai, L., & Tlili, I. (2023). Bioconvection flow of Cross nanofluid due to cylinder with activation energy and second order slip features. *Case Studies in Thermal Engineering*, 42, 102767.

72. Hussain, Z., Khan, W. A., Ali, M., Waqas, M., Kebail, I., & Abbas, S. Z. (2023).Chemically reactive magnetized tangent hyperbolic bidirectional nanofluid flow subject to interaction of gyrotactic moment of microorganisms and nanoparticles. *Tribology International*, https://doi.org/10.1016/j.triboint.2023.108659.

73. Li, S., Puneeth, V., Saeed, A. M., Singhal, A., Al-Yarimi, F. A., Khan, M. I., & Eldin, S. M. (2023). Analysis of the Thomson and Troian velocity slip for the flow of ternary nanofluid past a stretching sheet. *Scientific Reports*, 13(1), 2340.

74. Modi, K. V., Patel, P. R., & Patel, S. K. (2023). Applicability of mono-nanofluid and hybrid-nanofluid as a technique to improve the performance of solar still: A critical review. *Journal of Cleaner Production*, 135875.

75. Butt, Z. I., Ahmad, I., Shoaib, M., Ilyas, H., Kiani, A. K., & Raja, M. A. Z. (2023). Neuro-evolution heuristics for Prandtl-Eyring nanofluid flow with homogenous/heterogeneous reaction across a linearly heated stretched sheet. *Waves in Random and Complex Media*, 1-47.

76. Hosseinzadeh, K., Mardani, M. R., Paikar, M., Hasibi, A., Tavangar, T., Nimafar, M., & Shafii, M. B. (2023). Investigation of second grade viscoelastic non-Newtonian nanofluid flow on the curve stretching surface in presence of MHD. *Results in Engineering*, *17*, 100838.

77. Hamada, M. A., Khalil, H., Abou Al-Sood, M. M., & Sharshir, S. W. (2023). An experimental investigation of nanofluid, nanocoating, and energy storage materials on

the performance of parabolic trough collector. *Applied Thermal Engineering*, *219*, 119450.

78. Basit, M. A., Farooq, U., Imran, M., Fatima, N., Alhushaybari, A., Noreen, S., & Akgül, A. (2023). Comprehensive investigations of (Au-Ag/Blood and Cu-Fe3O4/Blood) hybrid nanofluid over two rotating disks: Numerical and computational approach. *Alexandria Engineering Journal*, *72*, 19-36.

79. Shah, Z., Shafiq, A., Rooman, M., Alshehri, M. H., & Bonyah, E. (2023). Darcy Forchhemier Prandtl-Eyring nanofluid flow with variable heat transfer and entropy generation using Cattaneo-Christov heat flux model: Statistical approach. *Case Studies in Thermal Engineering*, *49*, 103376.

80. Ullah, Z., Zaman, G., Ullah, I., & Makinde, O. D. (2023). Bioconvection flow of Prandtl–Eyring nanofluid in the presence of gyrotactic microorganisms. *ZAMM-Journal of Applied Mathematics and Mechanics/Zeitschrift für Angewandte Mathematik und Mechanik*, e202300358

81. Khan, M. R., Puneeth, V., Alqahtani, A. M., Alhazmi, S. E., Beinane, S. A. O., Shutaywi, M., & Alsenani, T. R. (2023). Numerical simulation and mathematical modeling for heat and mass transfer in MHD stagnation point flow of nanofluid consisting of entropy generation. *Scientific Reports*, *13*(1), 6423.

82. Hussain, M., & Sheremet, M. (2023). Convection analysis of the radiative nanofluid flow through porous media over a stretching surface with inclined magnetic field. *International Communications in Heat and Mass Transfer*, *140*, 106559.

83. Maranna, T., Sachhin, S. M., Mahabaleshwar, U. S., & Hatami, M. (2023). Impact of Navier's slip and MHD on laminar boundary layer flow with heat transfer for non-Newtonian nanofluid over a porous media. *Scientific Reports*, *13*(1), 12634.

84. Rehman, S., Eldin, E. M. T., Bafakeeh, O. T., & Guedri, K. (2023). Coupled energy and mass transport for non-Newtonian nanofluid flow through non-parallel vertical enclosure. *Ain Shams Engineering Journal*, *14*(8), 102023.

85. Rehman, S. U., Haq, R. U., Khan, Z. H., & Lee, C. (2016). Entropy generation analysis for non-Newtonian nanofluid with zero normal flux of nanoparticles at the stretching surface. *Journal of the Taiwan Institute of Chemical Engineers*, 63, 226-235.

86. Mabood, F., Abbasi, A., Farooq, W., Hussain, Z., & Badruddin, I. A. (2022). Effects of non-linear radiation and chemical reaction on Oldroyd-B nanofluid near oblique stagnation point flow. *Chinese Journal of Physics*, 77, 1197-1208.

87. Ahmed, J., Khan, M., & Ahmad, L. (2019). Stagnation point flow of Maxwell nanofluid over a permeable rotating disk with heat source/sink. *Journal of Molecular Liquids*, 287, 110853.

88. Khan, U., Zaib, A., Abu Bakar, S., & Ishak, A. (2022). Unsteady stagnation-point flow of a hybrid nanofluid over a spinning disk: analysis of dual solutions. *Neural Computing and Applications*, 34(10), 8193-8210.

89. Vijay, N., & Sharma, K. (2023). Dynamics of stagnation point flow of Maxwell nanofluid with combined heat and mass transfer effects: A numerical investigation. *International Communications in Heat and Mass Transfer*, 141, 106545.

90. Khashi'ie, N. S., Waini, I., Wahid, N. S., Arifin, N. M., & Pop, I. (2023). Unsteady separated stagnation point flow due to an EMHD Riga plate with heat generation in hybrid nanofluid. *Chinese Journal of Physics*, 81, 181-192.

91. Murad, M. A. S., Hamasalh, F. K., & Ismael, H. F. (2023). Numerical study of stagnation point flow of Casson-Carreau fluid over a continuous moving sheet. *AIMS Mathematics*, 8(3), 7005-7020.

92. Zainal, N. A., Waini, I., Khashi'ie, N. S., Kasim, A. R. M., Naganthran, K., Nazar, R., & Pop, I. (2023). Stagnation point hybrid nanofluid flow past a stretching/shrinking sheet driven by Arrhenius kinetics and radiation effect. *Alexandria Engineering Journal*, 68, 29-38.

93. Vishalakshi, A. B., Mahabaleshwar, U. S., Pérez, L. M., & Manca, O. (2023). Hiemenz stagnation point flow with computational modelling of variety of boundary conditions. *Journal of Magnetism and Magnetic Materials*, 575, 170747.

94. Makhdoum, B. M., Mahmood, Z., Fadhl, B. M., Aldhabani, M. S., Khan, U., & Eldin, S. M. (2023). Significance of entropy generation and nanoparticle aggregation on stagnation point flow of nanofluid over stretching sheet with inclined Lorentz force. *Arabian Journal of Chemistry*, 16(6), 104787.

95. Yu, Y., Khan, U., Zaib, A., Ishak, A., Waini, I., Raizah, Z., & Galal, A. M. (2023). Exploration of 3D stagnation-point flow induced by nanofluid through a horizontal plane surface saturated in a porous medium with generalized slip effects. *Ain Shams Engineering Journal*, 14(2), 101873.

96. Islam, A., Mahmood, Z., & Khan, U. (2023). Double-diffusive stagnation point flow over a vertical surface with thermal radiation: Assisting and opposing flows. *Science Progress*, 106(1), 00368504221149798.

97.   Naveed Khan, M., Abbas Khan, A., Wang, Z., F. Alrihieli, H., M. Eldin, S., Aldosari, F. M., & E. Elseesy, I. (2023). Flow investigation of the stagnation point flow of micropolar viscoelastic fluid with modified Fourier and Fick's law. *Scientific Reports*, 13(1), 9491.

98.   Pontin, D. I., Priest, E. R. (2022). Magnetic reconnection: MHD theory and modelling. *Living Reviews in Solar Physics*, 19(1), 1.

99.   Bafakeeh, O. T., Raghunath, K., Ali, F., Khalid, M., Tag-ElDin, E. S. M., Oreijah, M., & Khan, M. I. (2022). Hall current and Soret effects on unsteady MHD rotating flow of second-grade fluid through porous media under the influences of thermal radiation and chemical reactions. *Catalysts*, 12(10), 1233.

100.   Safdar, R., Jawad, M., Hussain, S., Imran, M., Akgül, A., & Jamshed, W. (2022). Thermal radiative mixed convection flow of MHD Maxwell nanofluid: implementation of Buongiorno's model. *Chinese Journal of Physics*, 77, 1465-1478.

101.   Patil, P. M., & Kulkarni, M. (2022). MHD quadratic mixed convective Eyring-Powell nanofluid flow with multiple diffusions. *Chinese Journal of Physics*, 77, 393-410.

102.   Amjad, M., Khan, M. N., Ahmed, K., Ahmed, I., Akbar, T., & Eldin, S. M. (2023). Magnetohydrodynamics tangent hyperbolic nanofluid flow over an exponentially stretching sheet: Numerical investigation. *Case Studies in Thermal Engineering*, 45, 102900.

103.   Boujelbene, M., Rehman, S., Alqahtani, S., Alshehery, S., & Eldin, S. M. (2023). Thermal transport and magnetohydrodynamics flow of generalized Newtonian nanofluid with inherent irreversibility between conduit with slip at the walls. *Engineering Applications of Computational Fluid Mechanics*, 17(1), 2182364.

104.   Rashid, A., Dawar, A., Ayaz, M., Islam, S., Galal, A. M., & Gul, H. (2023). Homotopic solution of the chemically reactive magnetohydrodynamic flow of a hybrid nanofluid over a rotating disk with Brownian motion and thermophoresis effects. *ZAMM-Journal of Applied Mathematics and Mechanics* https://doi.org/10.1002/zamm.202200262.

105.   Waini, I., Hamzah, K. B., Khashi'ie, N. S., Zainal, N. A., Kasim, A. R. M., Ishak, A., & Pop, I. (2023). Brownian and thermophoresis diffusion effects on magnetohydrodynamic Reiner–Philippoff nanofluid flow past a shrinking sheet. *Alexandria Engineering Journal*, 67, 183-192.

106.   Alrabaiah, H., Haq, I., Saeed, A., Dawar, A., Weera, W., & Galal, A. M. (2023). Generalized heat and mass transport features of MHD Maxwell nanofluid flows past a

linearly Bi-stretching surface in the presence of motile microorganisms and chemical reaction. *South African Journal of Chemical Engineering*, 43, 146-161.

107. Ragulkumar, E., Palani, G., Sambath, P., & Chamkha, A. J. (2023). Dissipative MHD free convective nanofluid flow past a vertical cone under radiative chemical reaction with mass flux. *Scientific Reports*, 13(1), 2878.

108. Mahmud, K., Duraihem, F. Z., Mehmood, R., Sarkar, S., & Saleem, S. (2023). Heat transport in inclined flow towards a rotating disk under MHD. *Scientific Reports*, 13(1), 5949.

109. Abbas, N., Shatanawi, W., Abodayeh, K., & Shatnawi, T. A. (2023). Comparative analysis of unsteady flow of induced MHD radiative Sutterby fluid flow at nonlinear stretching cylinder/sheet: Variable thermal conductivity. *Alexandria Engineering Journal*, 72, 451-461.

110. Zeeshan, Ahammad, N. A., Shah, N. A., Chung, J. D., & Khan, M. S. (2023). Computational and Stability Analysis of MHD Time-Dependent Thermal Reaction Flow Impinging on a Vertical Porous Plate Enclosing Magnetic Prandtl Number and Thermal Radiation Effect. *Mathematics*, 11(6), 1376.

111. Shahid, A., Bhatti, M. M., Ellahi, R., & Mekheimer, K. S. (2022). Numerical experiment to examine activation energy and bi-convection Carreau nanofluid flow on an upper paraboloid porous surface: Application in solar energy. *Sustainable Energy Technologies and Assessments*, 52, 102029.

112. Algehyne, E. A., El-Zahar, E. R., Elhag, S. H., Bayones, F. S., Nazir, U., Sohail, M., & Kumam, P. (2022). Investigation of thermal performance of Maxwell hybrid nanofluid boundary value problem in vertical porous surface via finite element approach. *Scientific Reports*, 12(1), 2335.

113. Arshad, M., Hussain, A., Hassan, A., Shah, S. A. G. A., Elkotab, M. A., Gouadria, S.,& Galal, A. M. (2022). Heat and mass transfer analysis above an unsteady infinite porous surface with chemical reaction. *Case Studies in Thermal Engineering*, 36, 102140.

114. Shah, S., Rafiq, N., Abdullah, F. A., Atif, S. M., & Abbas, M. (2022). Slip and radiative effects on MHD Maxwell nanofluid with non-Fourier and non-Fick laws in a porous medium. *Case Studies in Thermal Engineering*, 30, 101779.

115. Usafzai, W. K. (2023). Multiple exact solutions of second degree nanofluid slip flow and heat transport in porous medium. *Thermal Science and Engineering Progress*, 40, 101759.

116. Ullah, Z., Ahmad, H., Khan, A. A., Aldhabani, M. S., & Alsulami, S. H. (2023). Thermal conductivity effects on mixed convection flow of electrically conducting fluid along vertical magnetized plate embedded in porous medium with convective boundary condition. *Materials Today Communications*, 35, 105892.

117. Khan, M. N., Ahmed, A., Ahammad, N. A., Alqahtani, T., & Algarni, S. (2023). Insights into 3D flow of Casson fluid on exponential stretchable surface in rotating frame through porous medium. *Ain Shams Engineering Journal*, 14(2), 101849.

118. Awan, S. E., Ali, F., Awais, M., Shoaib, M., & Raja, M. A. Z. (2023).Intelligent Bayesian regularization-based solution predictive procedure for hybrid nanoparticles of AA7072-AA7075 oxide movement across a porous medium. *ZAMM-Journal of Applied Mathematics and Mechanics/Zeitschrift für Angewandte Mathematik und Mechanik*, https://doi.org/10.1002/zamm.202300043.

119. Abbas, A., Khandelwal, R., Ahmad, H., Ilyas, A., Ali, L., Ghachem, K., & Kolsi, L. (2023). Magnetohydrodynamic Bioconvective Flow of Williamson Nanofluid over a Moving Inclined Plate Embedded in a Porous Medium. *Mathematics*, 11(4), 1043.

120. Zhang, G., Zhang, R., Kong, Y., & Wang, F. (2023). Complicated hydrate formation kinetics induced by ion specific effect in porous surface. *Chemical Engineering Journal*, 467, 143471.

121. Tran, H. H., Lee, D., & Riassetto, D. (2023). Wetting ridges on slippery liquid-infused porous surfaces. *Reports on Progress in Physics*.

122. Dhivagar, R., Shoeibi, S., Parsa, S. M., Hoseinzadeh, S., Kargarsharifabad, H., & Khiadani, M. (2023). Performance evaluation of solar still using energy storage biomaterial with porous surface: An experimental study and environmental analysis. *Renewable Energy*, 206, 879-889.

123. Whitaker, S. (1977). *Fundamental Principles of Heat Transfer.* (1st ed.) United Kingdom.: Elsevier Science and Technology Books.

124. McDonald, A. T., Fox, R. W., and Pritchard, P. J. (2009). *Introduction to fluid mechanics.* (8th ed.) India.: Wiley

125. Musharafa (2021). *Lie group study of some non-newtanion fluid flow with heat transfer analysis.* MS Thesis pages 28-34, University of Engineering and Technology, Lahore.

126. Abdelmalek, Z., Hussain, A., Bilal, S., Sherif, E. S. M., & Thounthong, P. (2020). Brownian motion and thermophoretic diffusion influence on thermophysical aspects of

electrically conducting viscoinelastic nanofluid flow over a stretched surface. *Journal of Materials Research and Technology*, 9(5), 11948-11957.

127. Fathizadeh, M., Madani, M., Khan, Y., Faraz, N., Yıldırım, A., & Tutkun, S. (2013). An effective modification of the homotopy perturbation method for MHD viscous flow over a stretching sheet. *Journal of King Saud University-Science*, 25(2), 107-113.

128. Akbar, N. S., Ebaid, A., & Khan, Z. H. (2015). Numerical analysis of magnetic field effects on Eyring-Powell fluid flow towards a stretching sheet. *Journal of magnetism and Magnetic Materials*, 382, 355-358.